TOPIC: **THE EFFECTS OF A HYDRATE BLOCKAGE ON THE LAYERS OF A FLEXIBLE PIPE DURING PIGGING: CASE STUDY- GULF OF GUINEA**

AUTHORS: **Gbenga A. Owolabi**
Lead, Supply and Distribution Department
Petroleum Product Marketing Company (PPMC)-Nigerian National Petroleum Limited (NNPC Ltd) Lagos

Key words: *Non-bonded flexible pipes, Sample-A Blocked flexible pipe, Sample-B unblocked flexible pipe, Abaqus, pressurization, depressurization, pigging*

ABSTRACT

Generally, the blockages in an unbonded flexible pipe have over the years shown to be a problem, that needs a collective efforts to resolve. Thus, the behaviour of a non-bonded flexible pipes with blockage by hydrate, sand, and wax under the influence of various load conditions were studied and analyzed as reported in this paper. Non-linear tri-dimensional finite element models were used based on two (2) scenarios; blocked and unblocked conditions. The models recreate a seven (7)-layer flexible pipe with two tensile armour layers, an external polymeric sheath, high strength tape, orthotropic equivalent carcass, and pressure armour layers with an internal polymetric sheath.

Several studies were conducted to verify the influence of key parameters on the instability phenomenon when the flexible pipe is under hydrate blockage. The internal pressure and compressive loads were considered as amongst the parameters, in which their variation causes a significant change in the stability response of the pipe layers. This includes a detailed description of the finite element model and a case study where the non-bonded flexible pipe is blocked by methane hydrate. The procedure of this analysis is here described, along with the results.

For in-depth knowledge of hydrate formation and its consequences in flexible pipes, this work used ABAQUS, a standard finite element (FE), in modelling, simulating, and investigating a hydrate blocked and unblocked non-bonded flexible pipe under the influence of internal pressure.

A simplified model was employed and a finer mesh to resolve the issue with the FE model. And progress the effect of the hydrate on the pipe layers.

Importantly, this present work considered and investigated a 7-layers 6” diameter non-bonded flexible pipe as a case study. The results were obtained from the investigations, analyzed, and

presented accordingly. Obtained results showed a significant influence of methane hydrate on Sample A, while Sample B behaves normally under various load conditions.

INTRODUCTION

Considered in the study was a seven (7) layers non-bonded flexible pipe with a hydrate plug or blockage was created with a finite element software ABAQUS to model and simulate the behaviour. The effects of human activities and unknown degradation in the process of removing the plug through pressurization and depressurization process were evaluated, also the effects also create on the layers during regular pigging operation. Considering that the usual though normal operation as commonly carried out in oil and gas industries including any other pipes, have perhaps a long-time effect on the pipe.

This paper investigated the common but neglected or never thought effect of hydrate plug inside the flexible pipe length adopting the same methods by several researchers. In finite element model (FEM) model, the layers are modelled separately with different methods; the non - metallic layers were modelled in C3D8R solid element and S4R element cylindrical pipe with varying diameter but the same length of 2.8m. The metallic layers- Carcass, Pressure Armour and tensile wires were modelled the same solid and shell element to forms two models, while the equivalent materials, orthotropic using engineering constants was used to model the Carcass and Pressure armour, this is to have better and nearly accurate result according to [1]. The tensile wires were modelled as a revolved rectangular strip which were then assembled together based on the number of tendons in the case study. The model considered contact interfaces; interaction between layers and formulated the contact interaction, geometric nonlinearity, normal behaviour of stiffness and friction.

FLEXIBLE PIPES DESCRIPTION

A typical non-bonded flexible pipe comprises multiple layers made up of metallic and non-metallic materials, commonly used in transporting or extracting oil, gas and water due to their mechanical and chemical properties [2].

Flexible pipes exist as bonded and non-bonded systems with the principal difference in the vulcanization process. The bonded layers are joined and do not slip over one another while the layers are contacted and interact with friction in a non-bonded flexible pipe [3]. The ideal system would enable flexibility of the structure against wear and tear due to ocean conditions.

This paper presents an overview of the design and composition of layered pipes and their usage within the oil and gas industry and highlights the need for research to address hydrate blockage issues.

Flexible layers

Flexible pipes are made up of key layers, each of

which has a specific function or functions and are designed explicitly for a given application. Moreover, there is an extensive range of possible layer combinations dependent on the exact nature of the application.

Typical flexible pipe layers comprise of the following elements: the tensile armours, external sheath, pressure sheath, interlocked steel carcass and pressure armour, as shown in Figure 1. The arrangement and composition (number, type, and sequence) of the layers are dependent on the composition of the fluid and the requirements of the process application. The following section describes the rationale of the design approach for each layer and any relevant issues on the material and design approach for that sub-component.

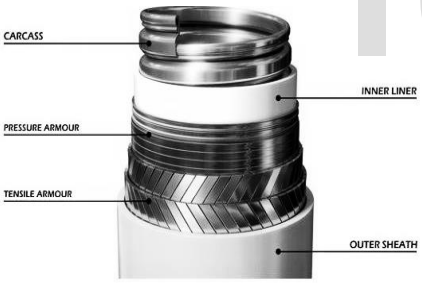

Figure 1: Non-bonded flexible pipe [2]

Carcass Layer

The collapse capacity of the carcass is determined by assuming that the external hydrostatic pressure is being applied directly to the inner liner to account that the pipe may be flooded because of a damaged outer sheath which could be determined through an annulus test. Generally, it is made from American Iron and Steel Institute (AISI) 304-grade stainless-steel by cold forming a flat stainless-steel strip to form an interlocked structure, as shown in Figure 2.

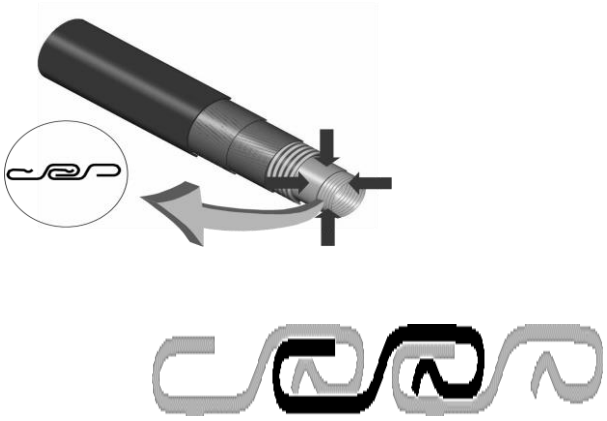

Figure 2: Conventional carcass structure for a non-bonded flexible pipe

Pressure Sheath

The pressure sheath is made of either High-Density Polyethylene (HDPE) or Cross-Linked Polyethylene (XLPE), Polyamide (PA11), or Polyvinylidene fluoride (PVDF), which is based on a solid extrusion hence, making it serve as leak-proof.

Depending on design requirements, a sizeable number of pressure sheath layers can act as leakproof for the flowing liquid or gas and give further protection to both the carcass and pressure armour layers. It is essential to consider the pressure build-up between the layers of a multi-layered inner liner caused by gas seeping through the carcass layer since it is not leak-proof. As shown in Figure 3, the pressure sheath determines the maximum allowable temperature of the flowing content, which is often between 60 and 140 °C. It is noted that the pipe under consideration for this research programme is made from polyamide and has a maximum allowable temperature of 80°C.

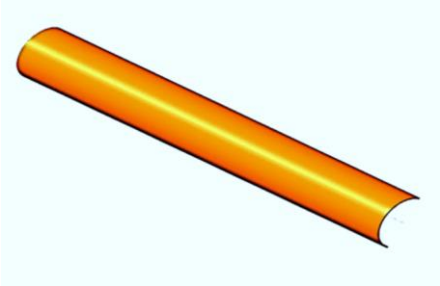

Figure 3: Showing the Pressure Sheath layer

Pressure Armour

This layer protects the flexible pipe against internal pressure due to hoop and radial stresses and protects against external hydrostatic. The pressure armour can also be designed to give the carcass layer additional support and increase the overall collapse capacity of the pipe. Figure 4 shows the interlocking wire profiles typically used, which is the wires that make up the pressure armour fabricated from low-alloyed carbon steels with a high yield strength between 850 and 1000 MPa.

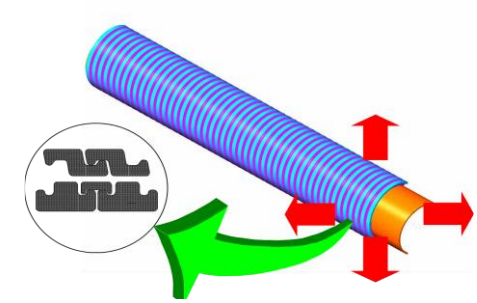

Figure 4: Typical pressure armour layer-interlocking wire profiles

Tensile Armour

Otherwise known as the tensile wires, this layer often consists of two (2) strips wounded in opposite directions, first and second tensile wires. However, this depends on the required configuration and customer demand. They provide strength in the axial direction of the pipe. The armour offers tensile strength capacity to help support the pipe weight and resist external tension and end cap loads. Like the pressure armour, it is made up of helically wound metallic wires, but with a relatively low lay angle, between 25 and 35°. The wires have a rectangular cross-section; however, round profiles may also be used depending on the application. Typical sizes can be 2 x 7 mm, as applicable in the present research, and 2.5 x 8 mm, 4 x 8 mm, 3 x 6 mm etc. and so on. The wires are cross wound in pairs to ensure the best possible torsional balanced design for the pipe. This means that axial tension or compression loads do not cause significant twisting or torsion on the pipe. They are made of low-alloyed carbon steel, with very high yield strength, typically between 700 and 1500 MPa, as shown in Figure 5.

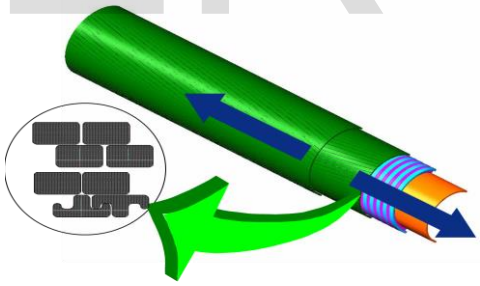

Figure 5: Tensile Armour layer

High Strength Tape (HST)

It is often placed around the tensile armour layer(s) to limit the radial displacement of the tensile wires. This tape is a must-have for pipelines designed for marine applications. The external hydrostatic pressure is so high that it can cause sizeable axial compression loads in the pipe. The hydrostatic pressure difference between the pipe bore and the

seawater determines the magnitude of this compression load. This compression load can cause a 'bird cage' failure, which is where the tensile wires relieve their compression stresses through radial buckling, causing the outer sheath to rupture. The tape is generally from a fibre-reinforced polymer material- Kevlar wound around the outermost tensile armour with a lay angle of 35°.

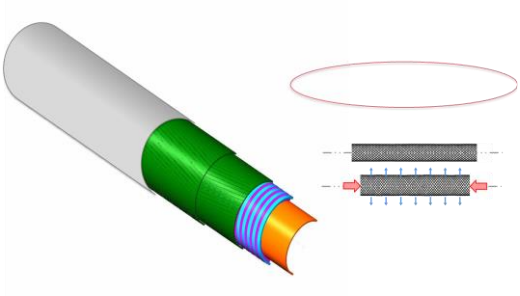

Figure 6: High Strength Tape

External Sheath

This layer protects the other layers, especially the armour steel, as it is in contact with the seawater, reducing the risk of corrosion and providing mechanical protection to the outermost tensile armour layer. It is like the inner liner, made from a solid extrusion of either polyethene (MDPE) or polyamide (PA11) material. MDPE is typically used in static applications, such as flowlines and jumpers, whereas PA11 is for dynamic applications, such as found in flexible pipes, due to its superior mechanical strength, as shown in Figure 7.

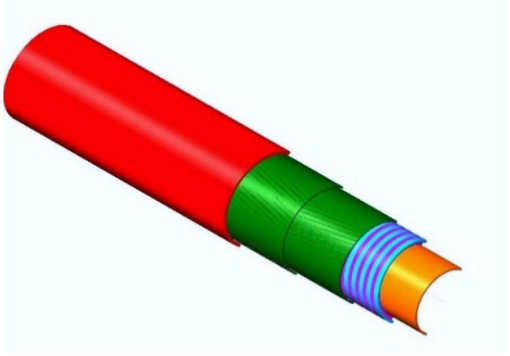

Figure 7: External Sheath layer

In the oil and gas industry, flexible pipes are specifically to transport oil, gas, and water in offshore deep or shallow waters, common between wells and floating production units or, in some cases, as an export line for offloading [6]. They have low bending stiffness and high axial stiffness, the reason for their flexibility in nature.

Consequently, the combination of flexibility and strength make the flexible pipes suitable for the highly dynamic conditions on the seabed with both metallic and non-metallic parts.

FLEXIBLE PIPES APPLICATION, HYDRATES, AND FAILURES

The applications of non-bonded flexible pipes in deepwater oil and gas production have witnessed tremendous growth since the 1990s because of their insulation properties, compatibility with chemicals, and flexibility against other available pipes [10]. They are commonly found in a water depth of around 2000 m; however, as the search for oil and gas goes deeper, there is an increase in the application of flexible pipes leading to changes in the technology to suit the requirements. Subsequently, General Electric (GE) has been

working tirelessly on better technology as demand increases. This includes adopting composite material layers to enhance the tension capacity and reduce the structure's weights [11]. The approach will enable the possibility of producing a multi-section pipe assembly to suit any client requirements.

In furtherance, studies have shown that flow assurance in flexible pipes has become an issue in offshore applications which requires proper attention. The flow is hindered by gas hydrates build-up that sometimes becomes enormous, complicated and impacts production operations. Hydrates are crystalline compounds like ice, composed of gas molecules trapped inside water molecules. And there are three (3) main types depending on the formation viz: Structure I (forms naturally), Structure II (forms in pipelines), and Structure H (forms in condensate) [12] [13]. The longer the flexible pipes, the probable the hydrated state is due to pressure drops along the length of the pipe. Chemical injection such as Thermodynamic Inhibitors (THI) prevents hydrate formation, as presented in Figure 8. Application of chemicals, though costly, can shift the equilibrium curve to more severe pressure and temperature conditions by allowing the pipeline to operate outside the hydrate forming region [14].

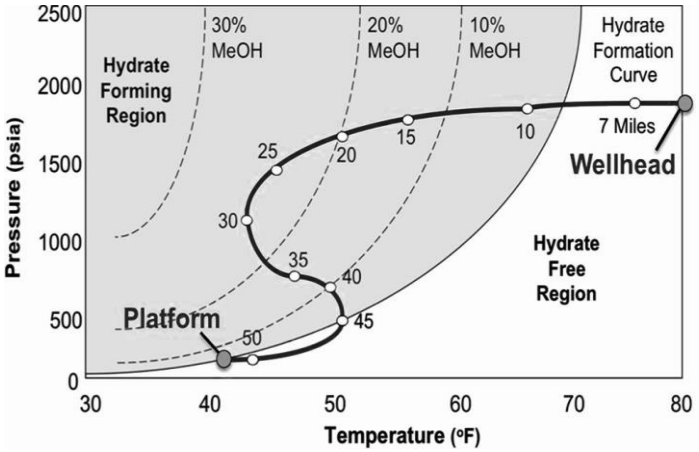

Figure 8: Pressure-Temperature curve of a field and hydrate forming boundaries methanol [11]

However, most major offshore fields around the world have experienced either mild or fatal subsea structures failures at a time in the life of the operations. So, in a wider range, there are flowline ruptures, riser failure, flowline blockage, SCM/SEM leakages, Umbilical failure, and fatigue of mechanical structures. However, it is well known that the deeper the offshore exploration, the higher offshore liabilities in term of failures. The failures are at alarming rates and have great impact on production.

Worldwide, the repair and replacement of damaged structures cost millions of US Dollars, often time leads to facilities shut down and production loss for a long period.

Today, many of such structures are undergoing repairs and root cause analyses. This is to determine the causes and mitigating factors/solutions while associated challenges include but not limited to the following:

- Flowline blockages

- Leakages of flanges at any point
- Corrosion of structures
- Umbilical leakages and discontinuity of cables and optic fibre
- SCM failures
- Obsolesce of the subsea structures etc.

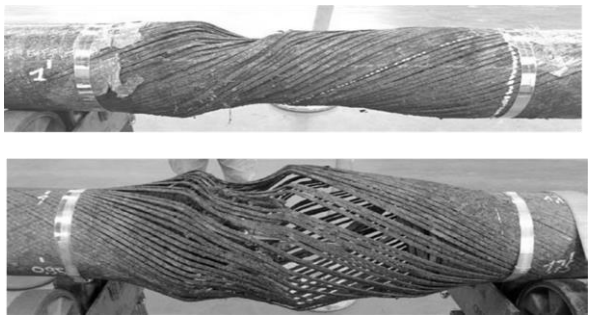

Figure 9: Flowline lateral and radial buckling and blockage

INTERNATIONAL OUTLOOK OF THE FLEXIBLE PIPE

More than 6000 flexible pipes have existed and deployed globally since 1974. Available records show that Brazil uses flexible pipes with over 2600, followed by the UK with over 800 and Norway with over 600 flexible pipelines fabricated and installed. Globally, Petrobras has 2570 units of pipes while BP is above 400 units in their fields [10].

In Africa, Angola is leading the usage of flexible pipes with almost 400 in operation and the reason a flexible pipe plant was established in the country by Technip. At the same time, Nigeria has over 200 confirmed flexible pipes of various lengths.

South America accounted for over 40% of the total flexible pipes manufactured and installed around the world. The pipelines have a pressure rating ranging from 0.7 to 103 MPa, with most non-bonded flexible pipes between 20.7 and 34.5 MPa. Although the pressure range has not changed significantly, the pressure rating for a given diameter was adjusted as required. The increase in diameter is due to larger extruders, and 1" pipes are almost extinct. So, the range now is 2" to 18" (ID), though the more significant part is within the range of 4" to 12" while 6" flexible pipe is the most demanded. The operating temperatures are in the range of -10 and 130°C, with over 40% of the flexible pipes operating at 80 and 90°C, although about 5% work above 100 to 130°C.

There is an increase in the flexible pipes demand annually, with the maximum demand between 2007 - 2015 compared to 1974 -1993 [15]. It shows the importance of the usage and the cost and maintenance advantages over rigid pipes.

It is noted that much have changed over the years in the production of flexible pipes in terms of usage, application, operational requirement, configuration, types, pressure ratings, internal diameters, and materials. The most significant change in flexible pipe applications is the operating water depth with 50% of currently deployed systems in less than 500 m while the remaining 50% are in greater depths, and it is increasing. About 15% of pipes are now installed in more than 2000 m water depth. As the increase in water depths raises concerns about overflow assurance challenges, the development of insulation and heating systems to prevent the flow challenges with new initiatives of replacing steel

tensile armours with similar rods carbon fibres are required.

Subsequently, more failures are recorded globally because of the increase in the number of flexible pipes.

The data used for this research was sourced from Technip, a renowned manufacturer of flexible pipes with over 80% supplying of global non-bonded flexible pipes. The outlook of flexible pipes usage globally is presented in Figures 10-19.

The outlook of flexible pipes usage globally and on a continent basis

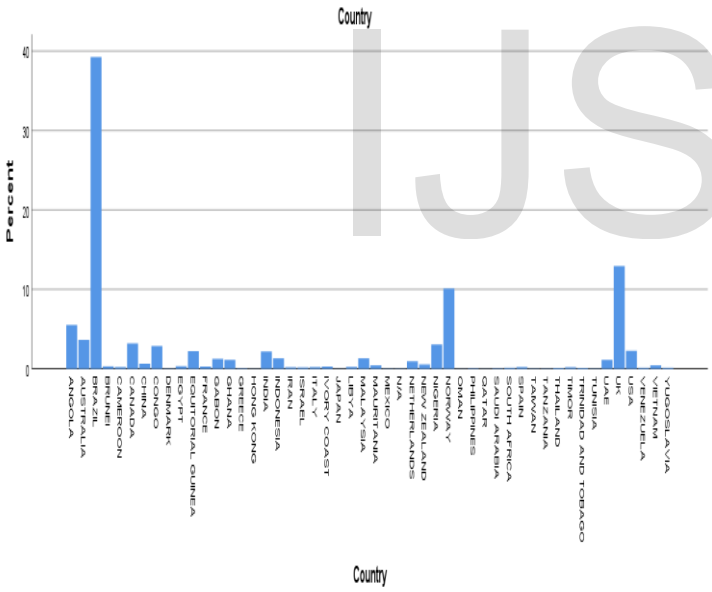

Figure 10: Flexible pipe usage

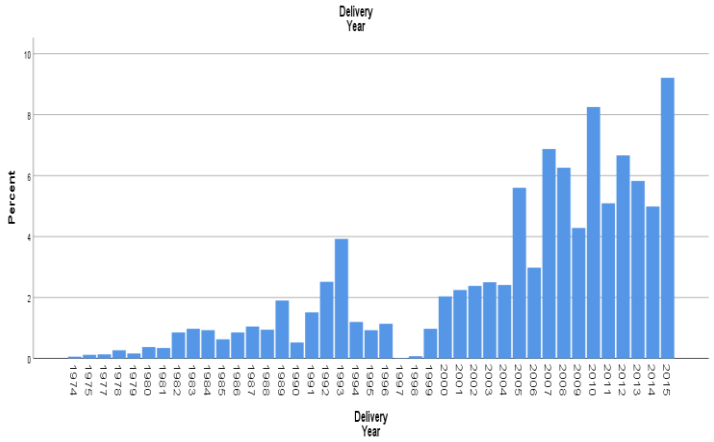

Figure 11: Flexible pipe usage yearly

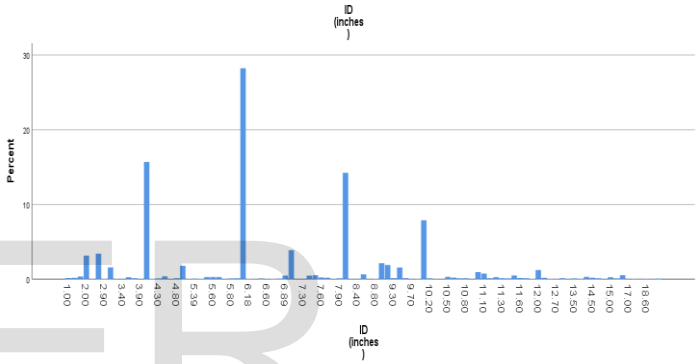

Figure 12: Flexible pipe size distribution and usage

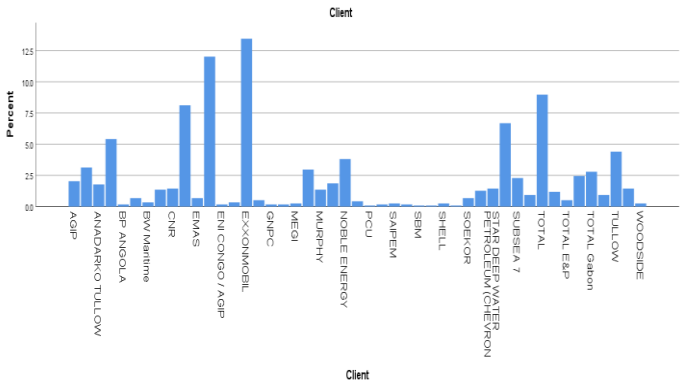

Figure 13: Flexible pipe usage based on Companies

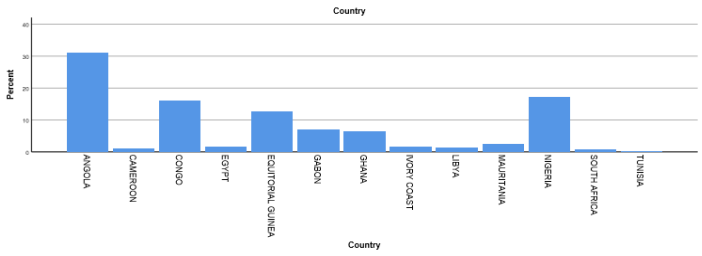

Figure 14: Flexible pipe usage in Africa

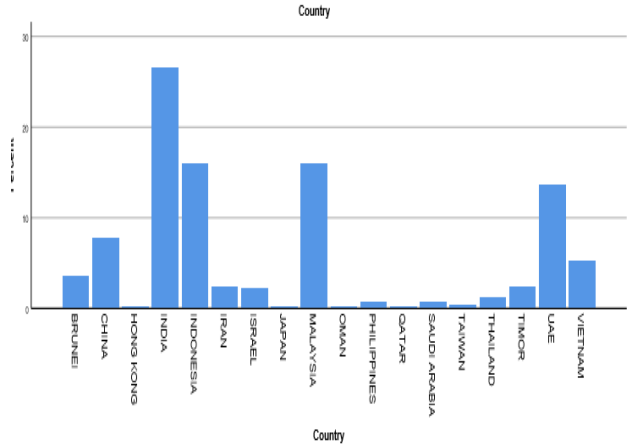

Figure 15: Flexible pipe usage in Asia

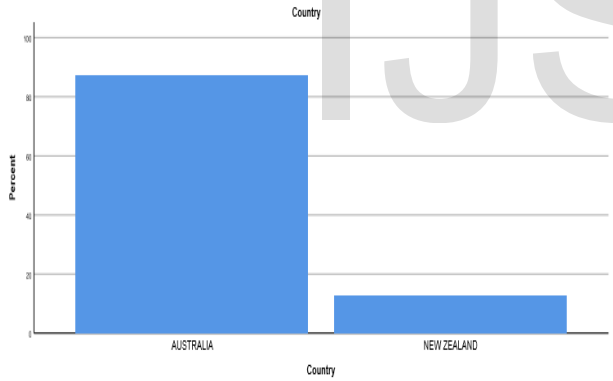

Figure 16: Flexible pipe usage in Australia

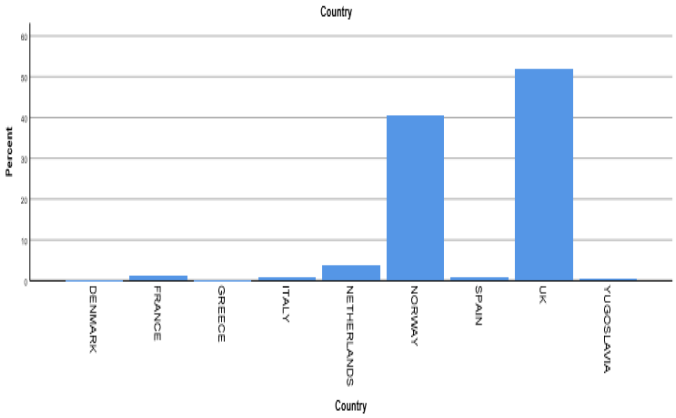

Figure 17: Flexible pipe usage in Europe

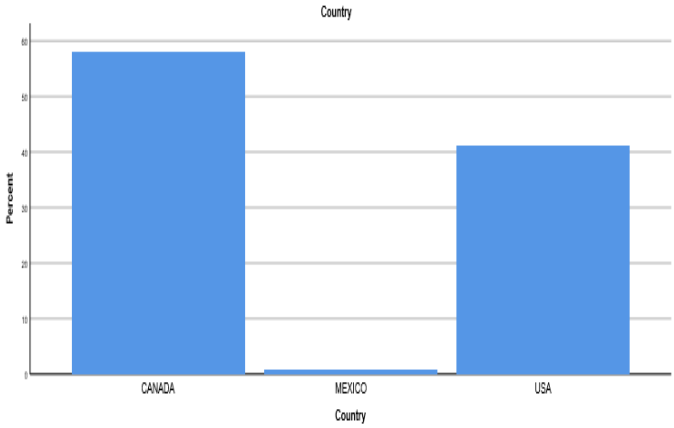

Figure 18: Flexible pipe usage in North America

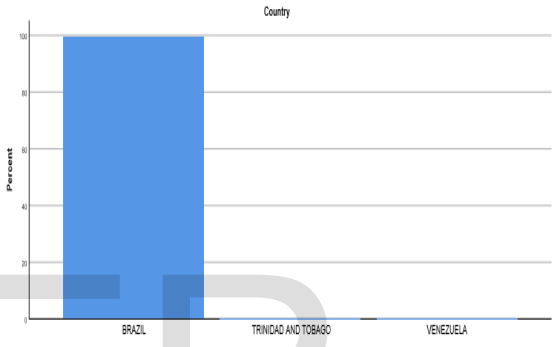

Figure 19: Flexible pipe usage in South America

PAST RESEARCH WORKS

Many modern engineering industries rely heavily on computational models for a multitude of purposes, primarily used for multiple types of complex failure analysis, additionally it is used heavily for optimisation with regards to design. Flexible pipes are no different, with computational analysis being the most widely used and important method in the field. This is primarily due to how efficient computational models are with regards to time and cost, mostly due to the huge advancements in modern day computational speed.

When it comes to computational and numerical analyses, the Finite Element Model (FEM) is one of the most flexible and useful for its ability to handle

complex 3D geometry, non-linear deformation and how two or more specific components work or "couple" together to share loads simultaneously and behave in unique ways. Additionally, different boundary conditions can be applied to FEM models allowing for a wider range of simulations.

Globally, a lot of works have been carried out in the experimental, numerical, mechanical, mathematical, and computational analyses of the non-bonded flexible pipes and all acknowledged.

However, less have been experimented in the analysis of hydrate/wax blocked non-bounded flexible pipes most especially those transporting gas were hydrate forms at high pressure and low temperature.

It is pertinent to know that during operation, the parameters employed in term of pressure, force and environmental factors have or may have adverse effect on the structure's layers with or without manufacturers guides. This commonly occurred during pigging or cleaning operation of a hydrate blocked pipe.

Subsequently, in the process of removing the hydrate, the pipes undergo pressurization and depressurization resulting to the expansion and contraction of the pipe based on hookes' law. This eventually led to certain failure mode as stated in API 7J [3] and API 7B [4] standard.

Detailed works carried out on flexible pipe research include but not limited to the following scientists such as Larsen et al [7] who conducted a cross comparison of results gathered from 11 different in-house programs from 20 of the most well-known academic institutions in the field. The study analysed the standard of computational methods for flexible pipe and prove consistency across the programs. The results gathered showed that static analysis of flexible pipes through computational methods was accurate to within 3% relatively solved showing strong correlations across all data sets. The dynamic analysis showed much less consistency with plus or minus 15 percent variation across results, estimated to be due to structural dampening and hydrodynamic loading. To minimise errors, benchmarking should be done for specific test cases in the future when using dynamic computational analysis for flexible pipe design. The main source of error from dynamic analysis is thought to come from how hard it is to accurately know specific seabed conditions as not all the information is known with regards to tidal conditions and variations, [7].

Ben Edmans, Dinh Chi Pham, Zhiqian Zhang, Tianfu Guo, Sridhar Narayanaswamy (2014)

Edmans et al. introduced a new multiscale approach for the analysis of FE flexible pipes. The primary focus is on the prediction of failure modes and increases in design life against hydrostatic loading. Dynamic research was conducted to find the displacements at specific points in the pipe, which was then emulated on more detailed local models. The author used a local model to help in predicting failure mechanisms, fatigue damage and buckling. The models were designed by first looking at

flexible pipes analytically as homogenized composite cylinders. Interlayer slip can be thought of as plastic flow through the homogenous material. A non-linear constitutive model (in structural mechanics, describe the relationship between strain or strain-like measures and stress or stress-like measures) can accurately mimic the behaviour of hysteresis bending in flexible pipes and shows the impact of internal pressure and hydrostatic loading as illustrated in Figure 2-1. This paper conclusively shows ordered multiscale designs for flexible pipe model, with evidence of hybrid beam FE implementation in a two-dimensional (2D) system. Accordingly, further works should be focused on "implementing a three-dimensional hybrid beam element and creating a fully nested computational procedure", with considerations of global and local systems.

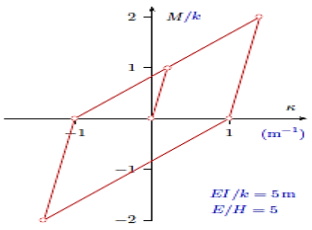

Figure 20: Bending Hysteresis loop obtained from Constitutive model [19]

The governing tangential bending stiffness under non-elastic loading/unloading is given in the following equation:

$$\frac{dM}{dk} = \frac{EH}{E+H} I \qquad \text{Equation 1}$$

where M is the bending moment, k is the curvature, E is the elastic material stiffness, H is the kinetic hardening modulus, and I is the second moment of area of the pipe [20]. However, the work is limited to 2D, which did not consider certain conditions.

Li, Qiu and Ju (2015)

Li, Qiu and Ju published a research article in 2015, which involved a 10-layer ABAQUS model that represented a non-bonded flexible riser. The analysis involved three different load conditions: tension, internal pressure, and external pressure. The model generation is well noted, with ten layers modelled individually considering friction, contact interaction, geometric non-linearity, and metallic (steel wires) interaction at specific layers. Presented is a typical section and model of carcass layers in Figure 20. This model's assumptions and attention to detail were impressive and a good benchmark for future ABAQUS work. The model used a mesh of 55000 elements and was solved using a modern-day eight (8) core CPU, with 24 Gb of memory. The model was limited to tension and pressure but did not consider the variation of other variables such as coefficient of friction, normal contact stiffness, and perhaps compressive force. If considered, the result would have been a good confirmation of flexible pipe-risers behaviour under different loads and boundary conditions.

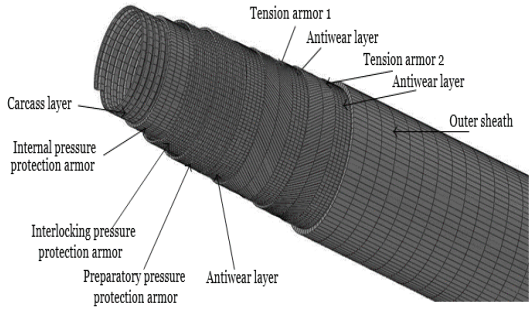

Figure 21: Ten layer's Riser [21]

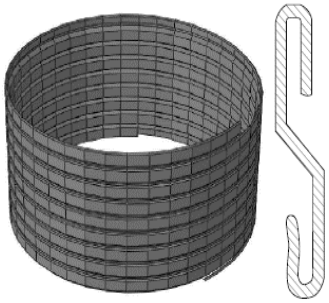

Figure 22: Section and model of carcass layer [21]

An FEA model was created, and all the layers were modelled separately, as shown in Figures 2-3 for the carcass layer. Appropriate contact interfaces were introduced between the layers to recreate a scenario like the flexible pipes. The specification of the riser layers is as detailed in Table 1.

Table 1: The specification of the riser layers used by J.Y Li and others [21]

Layer	Inner diameter (mm)	Thickness (mm)	Modulus (Pa)	Poisson's ratio (nu)	Density (ρ)
Inner carcass	178	3.5	207E9	0.30	7800
Internal Pressure armour	185	3.0	0.18E9	0.38	920
Interlock pressure armour	191	3.0	207E9	0.30	7800
Pre pressure armour	197	3.0	207E9	0.30	7800
Anti-wear tape 1	203	1.5	0.18E9	0.38	920
Tension armour1	206	2.0	207E9	0.30	7800
Anti-wear tape 2	210	1.5	0.18E9	0.38	920
Tension armour 2	213	2.0	207E9	0.30	7800
Anti-wear tape 2	217	1.5	0.18E9	0.38	920
Outer sheath	220	4.5	0.18E9	0.38	920
Length of pipe: 1.17m					

The mechanical behaviour of the model was evaluated under other loads and the three loading conditions: tension force, internal and external pressure. This paper is evidence that modern computational methods are continually improving and showing strongly correlated data for static loading or singular dynamic loading when compared to benchmarked experimental or analytical analysis. This shows a clear trend in this field of computational study of the non-bonded flexible riser, with the possibility of the problem being fully solved computationally in the future [22]

The results of the study shown in Table 2 based on load case-Tension of 150 kN were compared to analytical research showing a strong correlation, with enough data to validate the model.

Table 2: 10-layers flexible pipe model stress results

	Layers						
Stress	Carcass Layer	Internal Pressure protection Armour	Interlocking pressure protection armour	Preparatory pressure protection	Tension armour 1	Tension armour 2	Outer sheath
Von Mises Stress (MPa)	6.14	0.1104	14.32	19.61	98.48	91.51	0.1241

The analytical result obtained value of 87.01MPa is 11.7% and 4.9% smaller than the tension armour 1 and 2 simulation results 98.48MPa and 91.51MPa, respectively. This shows a good agreement between the analytical and numerical results. Other load conditions such as load case 2- Internal Pressure; load case 3-External Pressure also showed good understanding.

The model was revalidated, and the concept was considered in the actual work scenario due to its relationship with the loading conditions experienced by flexible pipes under blockage.

Conclusively, the model is relevant to this work as introducing hydrate into the model has significant differences in the stress values for the three load conditions.

The improvement is on introducing the Hydrate blockage and variation of coefficient of friction and stiffness constant, including the application of compressive force and longitudinal force already used.

Gabriel Gonzalez, Jose Renato Mendes des Sousa, and Luis Sagrilo (2015)

Gonzalez et al. presented a finite element model, entirely developed in ABAQUS® environment, fully capable of calculating stresses and strains in those several layers when subjected to different types of loads. The finite element model employs four nodes reduced integration shell elements. The inner layers, located below the first tensile armour, are condensed into a unique cylinder with its distinct properties well assured. The same assumption applied to the layers placed above the second tensile armour. Moreover, rebar elements were considered for the carcass and pressure armour modelling. As for the tensile armours, each steel tendon is modelled individually by shell elements. The interactions between tensile armours tendons and the tensile armours and the adjacent layers are handled with tangential and normal contact formulations. As a case study, a 9-layers 2.5" non bonded flexible pipe is considered under pure tension. The results are compared to an existing analytical model developed on six simplifying hypotheses and from previously published experimental data. All results agreed quite well but without hydrate blockage, which was studied in this work.

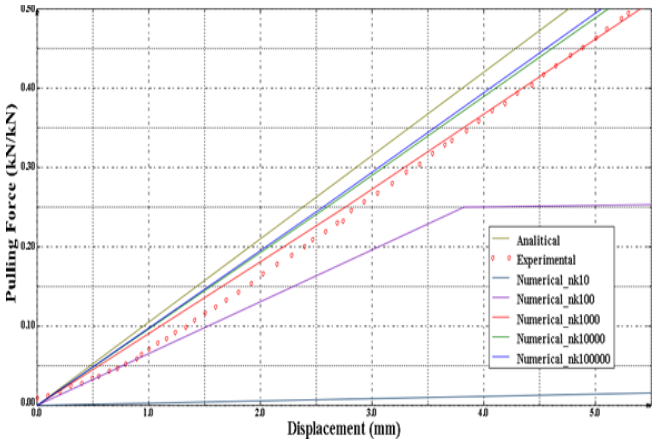

Figure 23: Displacement vs Pulling load for normal contact stiffness variation [2]

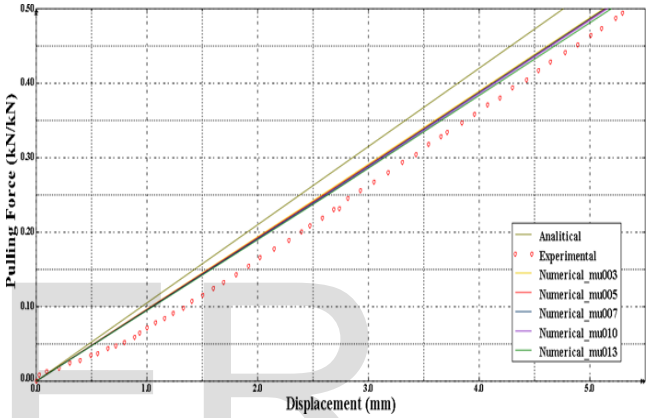

Figure 24: Displacement vs Pulling load for frictional coefficient variation [2]

The analyses considered the variation of normal contact stiffness (nk) and coefficient of friction (μ) which were chosen from 10-10^5 (μ = 0.10) and 0.03-0.13 (nk= 5000) for Normal stiffness and coefficient of friction as illustrated in Figures 23 and 24 respectively. The same model was verified and served as the basis for the developed models for this present work, including hydrate layer and other boundary conditions. In conclusion, the obtained results in numerical analyses varied with the analytical result. The numerical model depends on contact stiffness. This generates a model without physical correspondences if the value of stiffness is

not well chosen. The best parameters that give the desired result are when the friction coefficient is 0.10 and contact stiffness is 1000 N/mm^3.

J. de Sousa, Paulo F. Viero, Carlos Magluta N. Roitman and R. Motta. (June 2010)

De Sousa et al. dealt with a nonlinear three-dimensional finite element (FE) model capable of predicting the mechanical response of flexible pipes subjected to axisymmetric loads focusing on their axial compression response. Moreover, to validate the model required experimental tests, which were carried out at COPPE/UFRJ. In these tests, a typical 4" flexible pipe was subjected to axial compression until it failed with radial and axial displacements measured and compared to the model predictions. The excellent agreement between all obtained results indicates that the proposed FE model efficiently estimates flexible pipes' response to axial compression. Furthermore, it can potentially be employed in identifying the failure modes related to excessive axial compression and the mechanical analysis of flexible pipes under other types of loads.

De Sousa conducted axial compression experiments on a 4" flexible pipe, measuring the displacement under varying loads. The pipe is like the one analyzed in this project but of a different diameter. The experiment results could therefore be helpful in the verification of an FEA model; however, this project does not concern axial loading conditions. The axial shortening of the pipe specimen under varying load is shown in Figure 25.

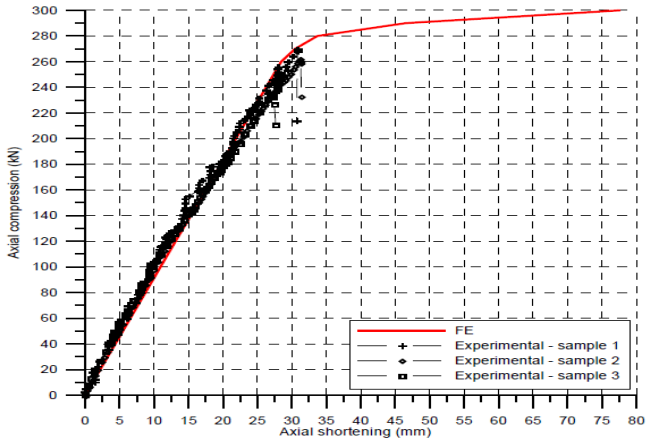

Figure 25: Axial Shortening of Flexible Pipe Under Axial Compression [23]

The results may not be accurate based on certain assumptions in the model, which includes but are not limited to:

1. The internal friction in the layers is negligible
2. No interaction between the laying direction of the tendons and their usual direction.
3. The thickness of the inner carcass and pressure armour is small compared to the internal diameter of the layers

Though the approach hypothesis as claimed may not have a significant effect on the results but was taken into consideration in the model of this present work.

Xu Yang, Svein Sarvik and Liping Sun (2015)

Yang et al. stated that the flexible pipes might be exposed to high axial compression and bending during deepwater installation. The compression force is mainly sustained by the tensile armour layers, resulting in localized lateral or radial buckling failure in these layers. This paper created a finite element model to evaluate the critical instability load of tensile armour wires under external pressure

and compression using different software such as Abaqus, Bflex, Bflex2, and M.A. Vaz. The tensile armour wires are modelled by curved beam elements under loxodromic (rhumb line) assumptions. Spring elements and equivalent beams simplified other layers' contributions. The buckling load capacity and associated failure modes are obtained. The results are also compared with the results based on 3D Euler beam elements and results published in the literature. Parametric analyses were further included with the external pressure, friction modelling and the influence of initial imperfections. The simulation results for different software are presented in Figures 26, 27 and 28.

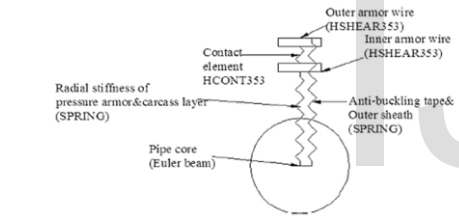

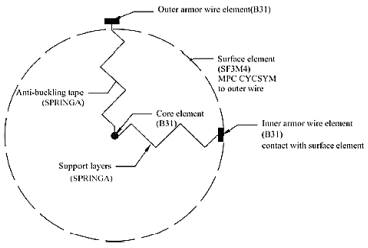

Figure 26: Schematic diagram of curved and straight beams models [24]

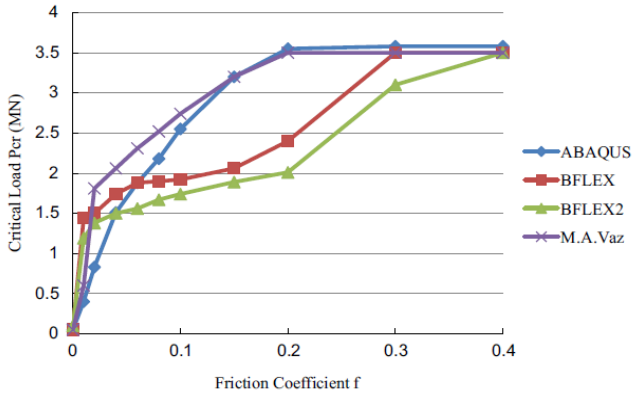

Figure 27: Critical load in different coefficient of friction at a pressure of 2MPa [24]

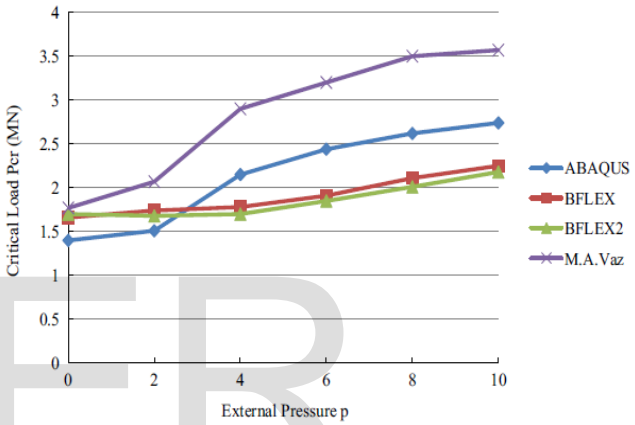

Figure 28: Critical load in different pressure at the coefficient of friction of 0.04 [24]

Analytical Analysis

Analytical models are the foundations of all engineering, as mathematics has been around for thousands of years with uses in engineering throughout history. Analytical modelling of flexible pipes is the oldest and most widely used method before modern computational advancements and accurate FE models. However, the basis of many FE models is a solid analytical model. The most common form of analytical modelling is to treat flexible pipes as cross-sectional models or composites. This method assumes that the pipe is not homogenous and is made of many different

unique parts. The model can then predict the behaviour of the pipe by summing the values of the "composite". This method simplifies the problem significantly; however, the ability to analyse individual components or the effects acting between layers. This simplified analysis gives only the overall macro properties of the pipe.

In contrast, more complex multi-layer analysis is often done with different properties and degrees of freedom assigned to each layer. This gives a more detailed, physically representative look into the micromechanics of flexible pipes. This section discusses analytical models and their pros and cons.

McIver (1995)

The paper presented the analytical basis used to model the complex behaviour of the individual components of the flexible pipe, which was employed to model the intricate details and structural behaviour of both non-bonded and bonded flexible pipes. Homogenous layers were represented as thick-walled cylinders while multiple loads were considered; "tension, torque, shear forces, bending moments, wall pressure.

Temperature pressure differentials, friction effects were monitored, and curvatures were noted. The model represented helical wires with beam elements, using Love's equations for equilibrium balancing and kinematic analysis. Serret-Frenet Formulae was used to transpose geometric data, to relate data to the flexural axis. Slippage is considered through material stresses and wire loading. The program "FLEX-ABLE" was developed based on the analytical findings, which reasonably predict axial loading. There were vital signs of coupling between most of the Degree of Freedom (DoF). Until this point (1995), programs available and made were not accurate enough to simulate this complex interactivity between multiple DoF, so there was a basis for future work. The Coulomb friction model should also be considered for future models to predict fatigue; however, this would require more detail for individual components in each layer of the analytical model [25].

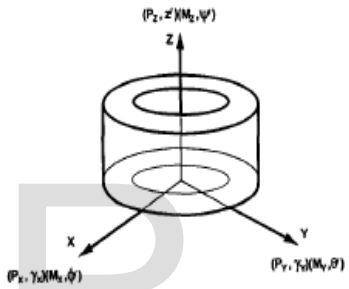

Figure 29: Pipe section load and deformation convention [25]

The pipe model applies to a total length, dZ, subjected to an axial tension Pz, torque Mz, shear force components Px and Py, bending moment components Mx, and My, pressure and temperature differentials through the pipe wall. The coordinate axis Z is directed along the pipe axis, as shown in Figure 2.10. The pipe section, and therefore each layer in the area, undergoes uniform axial strain z', shear deformations in the X-Z and Y-Z planes. They are represented by the shear angles x and y, bending curvatures about the pipe X and Y axes, respectively.

Roberto Ramos Jr. and Alexandre Kawano (2015)

This paper analyzed numerically a 2.5" flexible pipe subjected to traction and internal pressure. The effect of internal and external pressures on the displacement of flexible pipe, when subjected to axisymmetric loads, was discussed. A typical example is presented in Figure 30. The paper went further to derive the linear operators, which established the relationship among the stress resultants, displacements, or deformations in the individual layer of the flexible pipe, along with the process of deriving an analogous linear operator to represent the response of the entire flexible pipe. These are presented, highlighting interest, measured aspects, and their related meaning.

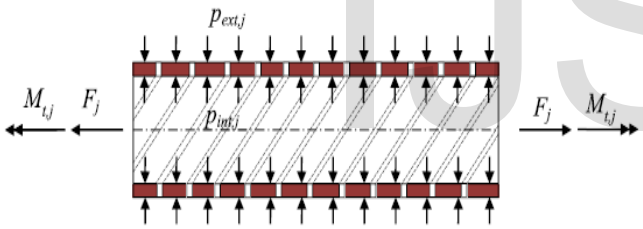

Figure 30: Load applied to the boundaries of a generic plastic layer [26]

- Traction force supported by the layer (F_j)
- Twisting moment supported by the layer (M_{tj})
- Internal pressure applied on the internal cylinder surface (p_{intj})
- External pressure applied on the internal cylinder surface (p_{extj})

The internal and external pressures applied to the respective cylindrical surfaces of the j-th layer can be related to stress-resultants F_{ipj} and F_{opj} (per unit of pipe length) defined respectively by:

$$Fipj = 2\pi Rij.\, Pintj \qquad \text{Equation 2}$$

and

$$\mathrm{Fipj} = 2\pi \mathrm{Rij}.\, \mathrm{Pintj} \qquad \text{Equation 3}$$

It is also important to stress that the internal and external pressures applied to the respective surfaces of the cylindrical layer are related to the contact pressures by:

$$\mathrm{Pintj} = \mathrm{Pcj} - 1 + {}^{\mathrm{n}}\mathrm{j}, \mathrm{int}.\, \mathrm{Pi} \qquad \text{Equation 4}$$

$$Pextj = Pcj - 1 + {}^{\mathrm{n}}j, ext.\, Po \qquad \text{Equation 5}$$

where Pcj is the contact pressure between the j.th and the (j+1)-th layers and is a flag that returns "1" if the layer is the minimum innermost waterproof layer of the pipe internal pressure Pi. This was applied in this work in terms of subjected loads [26]. The research is only limited to pressure, while other load conditions were not considered.

R. Cuamatzi-Melender, O. Castillo-Hernandez, A.O. Vazquez-Hernandez et. al (2017)

This work presents analytical and finite elements modelling strategies to study both types of collapse risers fabricated with an "S" carcass profile to predict collapse failure, as presented in Figure 2-12. The developed methodologies were applied to a 50.8 mm (2 in.) non-bonded flexible riser. The results showed the importance to perform 3D finite element modelling for a proper carcass design and collapse assessment, calibration of the length of the finite element models, and boundary conditions defined to obtain reliable results and computer time optimization. It also finds a difference in collapse

loads for each type of collapse; ovality type collapse, and the development of a finite element of the carcass only is sufficient. But for the other types of failure, it is necessary to develop a finite element model including carcass, internal polymer sheath and pressure armour. Furthermore, it was found that the analytical formulations developed to date can only evaluate the collapse properties of the carcass. Still, they are limited to being used to design carcass for flexible risers [27].

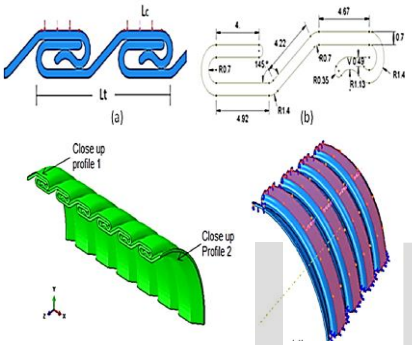

Figure 31: Typical Design of Carcass Layers [27]

The paper focused and limited the simulation to only the carcass layer, while the limited study was on other layers. The stress-strain carcass and sensitivity analysis are presented in Figures 31 and 32.

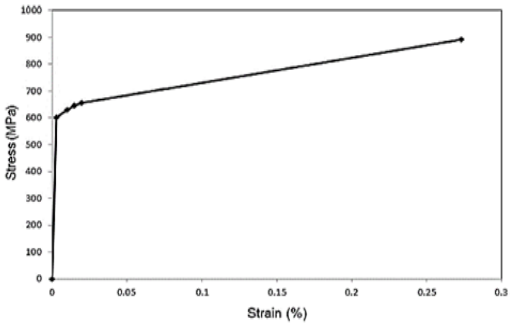

Figure 32: Sensitivity analysis maximum Von Mises Stress [27]

In conclusion, the study only considered the carcass layer, which limited understanding of the behaviour of other layers with the same load conditions.

Niels Højen Østergaard, Anders Lyckegaard, Jens H. Andreasen

The paper analysed lateral wire buckling in helical tensile armour layers. The study looked at understanding the effects of extreme deep-sea conditions. At these depths' pipes can undergo cyclic bending forces from tidal currents and experience axial compression. Flexible pipes are better for tensile forces; the tendons pull tightly together under tension, becoming slightly straighter and sitting in a more axial orientation. This increases their tensile axial load capacity; however, in compression, the tendons are pushed together, lowering the lay angle and causing their orientation to move more in the hoop direction than the resting state. This makes their ability to handle compression worse, and in extremes, can cause bird caging and structural failure. A spiral model was developed using thin curved beams (Figure 33), with a frictionless surrounding layer, using these single helical wires could be studied. The model's equations used curved beam equilibrium and compared different beam model sizes, validating results through multiplicative use through computational comparison, from these force-displacement graphs were obtained.

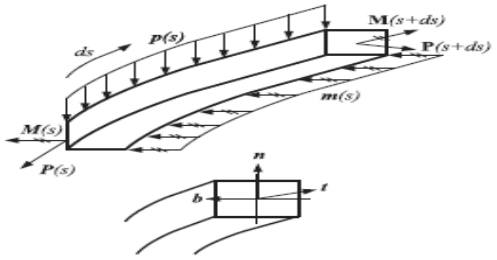

Figure 33: Curved beam equilibrium [28]

Component wise equations of equilibrium as derived by Love; the expressions (a power law) as shown below:

$$\left(\frac{dPt}{dS}\right) - KnPn + KgPb + pt = 0 \quad \text{Equation 6}$$

$$\left(\frac{dPn}{dS}\right) + KnPt - \tau Pb + pn = 0 \quad \text{Equation 7}$$

$$\left(\frac{\mathrm{dPb}}{\mathrm{dS}}\right) - \mathrm{KgPt} + \tau\mathrm{Pn} + \mathrm{Pb} = 0 \quad \text{Equation 8}$$

$$\left(\frac{\mathrm{dMt}}{\mathrm{dS}}\right) - \mathrm{KnMn} + \mathrm{KgMb} + \mathrm{mt} = 0 \quad \text{Equation 9}$$

$$\left(\frac{\mathrm{dMn}}{\mathrm{dS}}\right) + \mathrm{KnMt} - \tau\mathrm{Mb} - \mathrm{Pb} + \mathrm{mn} = 0 \quad \text{Equation 10}$$

$$\left(\frac{\mathrm{dMb}}{\mathrm{dS}}\right) - \mathrm{KgMt} + \tau\mathrm{Mn} + \mathrm{Pn} + \mathrm{mb} = 0 \quad \text{Equation 11}$$

The results showed that the pitch of the helical layers was the most crucial parameter for axial loading. As the pitch increases, the axial loading lowers significantly. There is not much research into slip mechanics, and future work should focus on lateral wire buckling with slip considered [28]

J.A Witz

Witz conducted a study into the response of flexible pipelines under various loading conditions. He then compared his results with the analytical solutions provided by ten (10) well-known institutions, including Lloyds Register, Statoil, and University College London (UCL). Some institutions chose to use purely mathematical models, while others used computer simulation software. The pipe used in the study was a 2.5" version of the pipe, and the participants were required to calculate the following curves for deformations within elastic limits:

1. Tension-axial elongation curve and twisting angle-axial elongation curve with ends free to rotate
2. Tension-axial elongation curve and twisting moment-axial elongation curve with ends prevented from rotating
3. Clockwise and anti-clockwise twisting moment-twisting angle curve and axial force-twisting angle curve with ends free to elongate
4. Clockwise and anti-clockwise twisting moment-twisting angle curve and axial force-twisting angle curve with ends prevented from moving axially
5. Bending moment-curvature curve for two internal gauge pressures of zero and 300 bar.

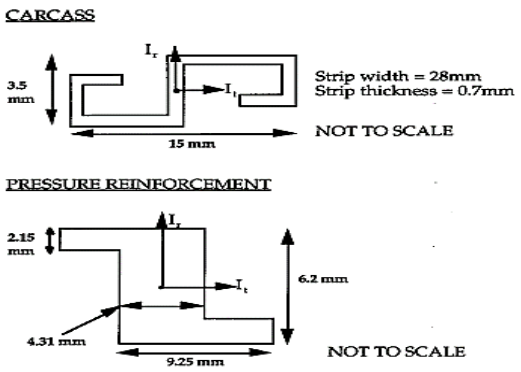

Figure 34: Carcass and Pressure reinforcement layers [29]

Figure 34 presents the mean axial force-elongation curve and the curves associated with stiffnesses one standard deviation on either side of the mean stiffness. Also shown in Figure 35 is the measured axial force-elongation curve for the first three load

cycles. The measured curve shows noticeable non-linearity with hysteresis in the loading cycle. Also evident is the difference between the first and subsequent load cycles. This is observed with non-bonded flexible structures and is commonly attributed to the bedding of the component layers. All models used in this case study, apart from the Coflexip model, predict axial stiffnesses larger than the measured axial stiffness.

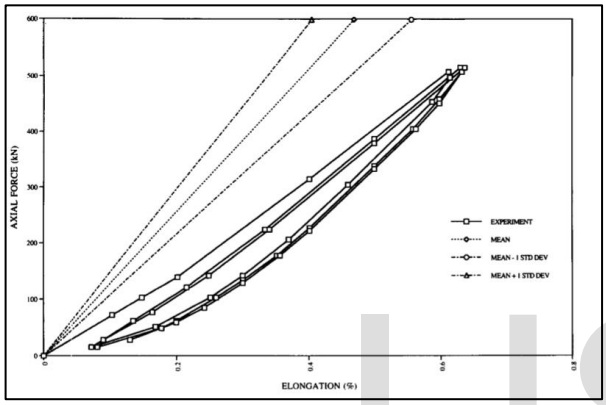

Figure 35: Cross-section analysis: Axial force/Elongation curve [29]

Additionally, the pipeline displayed a non-linear deformation with a degree of hysteresis after the initial loading. The mean value for stiffness provided by the ten institutions was significantly higher than was measured during the tests. The force divided by the strain of the pipeline was approximately 80MN. Coflexip, who used the Eflex software, were closest to the experimental result and calculated a value of 89MN. The mean value provided by the institutions was 128 MN, with UCL calculating a value more than double the value measured was the closest experiment. This shows that accurately modelling the behaviour of a non-bonded, layered, flexible pipe is a complex process. The study recommended further research to establish the structural behaviour of the flexible pipes under combined load, which is being investigated in this work. The loads recommended were applied to the model, which includes axial load. Figure 35 is a typical plot for the cross-section analysis of flexible risers.

Experimental analysis

The numbers of experimental published studies are relatively low compared to Analytical and Numerical studies. This might be due to the challenges and expenses required to set up the facilities necessary to carry out tests and analysis. Few reviews associated with the experimental study are presented below:

M. T. Rahmati, S. Norouzi H. Bahai and G. Alfano (2017)

This paper investigated a 4-layer flexible pipe which was examined through both experimental and numerical methods. The practical test was carried out on an adjustable riser to determine its responses when subjected to specific load conditions, and FEA was used to validate the results. The composition of the layer is two cylindrical polycarbonate tubes and two steel helical wires, and the helical is the carcass and tendon armour layers. Investigation with a bending load was carried out on the model and provided helpful information on the behaviour of flexible pipe and its structures and subsequently performed the finite element models with all layers modelled separately and applied a surface-to-surface frictional contact interaction. The

results comparison was finally made and predicted the responses of the investigated flexible pipe.

Experimental tests were to predict the flexible pipe nonlinear structural response. The riser consists of four layers which include two cylindrical polycarbonate tubes and two steel helical layers. One helical layer represents the carcass layer in a flexible riser, while the other represents the tendon armour layer.

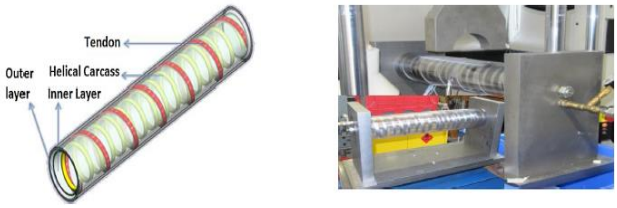

Figure 36: Assembly of prototype layers and specimen for bending test [30]

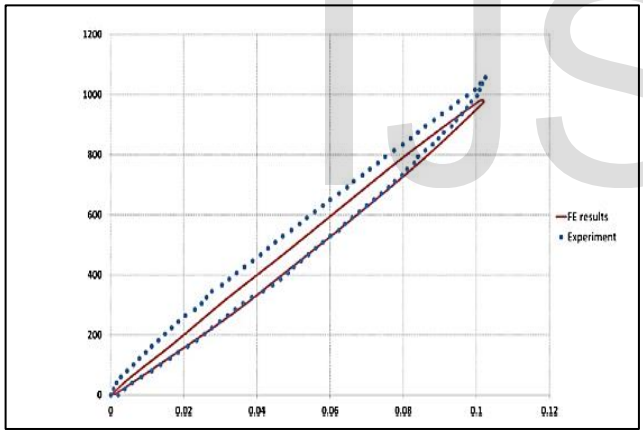

Figure 37: Predicted bending moment (N.m)-curvature (1/m) [30]

First, bending load experiments on the model are described, which provide some insight regarding the fundamental behaviour of flexible pipe structures (Figure 37). The description of the FE models follows this. All layer components are individually modelled, and a surface-to-surface frictional contact model is used to simulate their interaction. Finally, the FE numerical results were compared with the test data to outline the capacity of the numerical method to predict the response of flexible riser structures. Still, not all the results agreed both experimentally and numerically. This makes the authors suggest further investigation in the evaluation of various contact modelling approaches.

S. Péronne, Cecile Izarn, Pascal Estrier, Olivier Caro, Jean-Narc Leroy et al. (2015)

Péronne et al. performed research on hysteric bending behaviour in flexible pipes, with experimental characterization and FE analysis. Over 50 tests were run on a full-scale flexible pipe, with a focus of the studying being on how internal pressure affects bending behaviour. The inclusion of tension, external pressure, and temperature were considered in the setups. The setup is as presented in Figures 38 and 39.

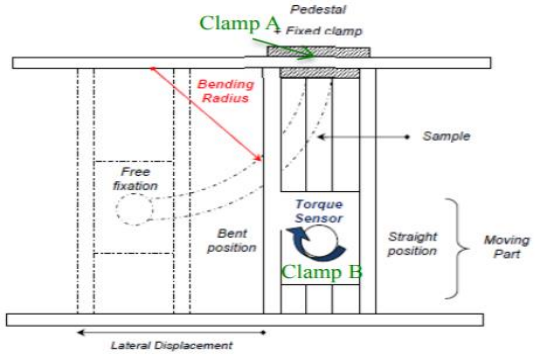

Figure 38: Bending characterization test-Sketch instrumentation [31]

Potentiometers were placed evenly along the pipe to record curvature time evolution, with strain gauges and torque sensors used at each end of the test specimen. The conditions used attempted to simulate a deep-sea condition with a water depth of 2000 m, as this is where most flexible pipes are used

in practicality. The results showed "the bending stiffness is much lower than its torsional and axial stiffnesses and therefore has a larger influence on its static and dynamic behaviour.", additionally the experiment showed linear bending stiffness is only affected by thermal loading. An FE design program, "STIFFNESS" based on IFPEN Life6, was presented, explicitly considering the tensile armour's layers effects on bending. The static outcomes were compared with the experimental results to show a strong correlation. Some slight differences were found when comparing uncertainties in global stress results, and dynamic tests do not show promising results. As the model generated is shown to be a reasonable overall predictive model, it should be helpful for future fatigue and high-stress failure analysis studies [31].

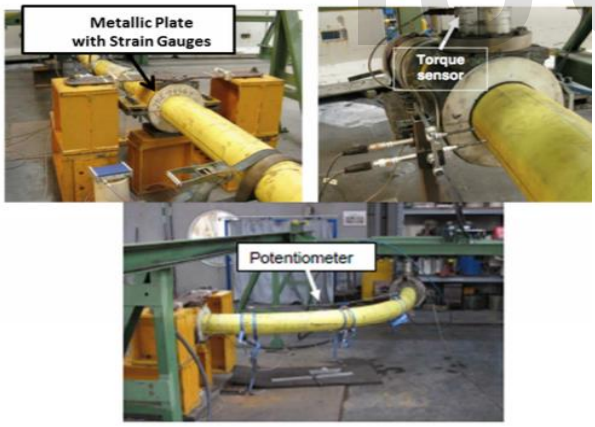

Figure 39: Characterization Test-Instrumentation [31]

Research Review on Hydrate Formation

Gas hydrates are solid crystalline compounds resembling ice in appearance, consisting of the main water lattice, the host, and individual gas molecules, the guests. The structure of these gas hydrates is determined by the size and composition of the gas molecule captured by the water lattice. The most common types of "guest" gas molecules are methane, ethane, propane, carbon dioxide, and hydrogen sulphide, as illustrated in Figure 40. Gas hydrates form when water and these gases become mixed in conditions with low temperature, generally below 25°C, and high pressures, usually greater than 1.5 MPa for natural gas hydrate formation. The two most common types of naturally occurring gas hydrates are structure I and structure II, as shown in Figure 40.

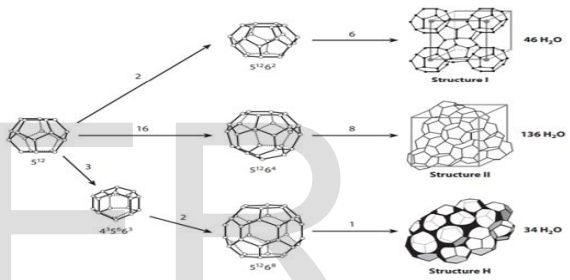

Figure 40: Three common hydrate unit crystal structures [32]

Gas hydrate formation becomes an issue in gas pipelines, particularly in subsea pipelines where the temperature and pressure conditions are ideal. The gas hydrate formation depends upon the needs of low temperature, high pressure, and the composition of the water-vapour mixture. Once these conditions are met, the gas hydrate formation can be accelerated through high-velocity flow streams and pressure pulsations. The hydrate formation can be considered a problem for oil and gas pipelines. Due to their solid crystalline form, they are non-flowing and build up in the pipeline

until the pipe becomes plugged. This can be seen in Figure 41.

Removal of these hydrate blockages. Once they have occurred, it can take time, sometimes several months, leading to costly production stoppages. Several options are available to achieve this; one is a pigging operation, which can only be undertaken if the flow is possible in the pipe. A 'pig' is a device inserted into the pipeline and can sweep away any blockages. Another method is depressurization of the pipeline, which aims to dissociate the hydrate from the pipe wall. However, this takes time and can be dangerous as a dislodged hydrate plug can cause damage to the pipeline. And finally, the hydrate can also be heated to dissociate the hydrate, but this can lead to rupture of the pipe if the gas hydrate expands.

Therefore, rather than shutting down a pipeline to remove a hydrate plug, it has generally been preferred to find ways of preventing the formation of gas hydrates within pipelines. Four techniques that have been used to avoid the appearance of hydrates are as follows.

1. Remove the free and dissolved water from the system with separators, glycol dehydrators, molecular sieves, or other methods.
2. Maintaining temperatures above the range in which hydrates can form.
3. Maintaining low pressures to keep all phases fluid.
4. Injecting an inhibitor to prevent the formation of hydrate. An inhibitor is a substance that slows down or stops a chemical reaction or a process or reduces the activity of a reactant, catalyst, or enzyme.

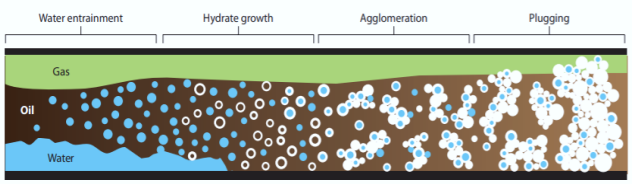

Figure 41: Gas Hydrate Build-up in Pipeline and Eclipse pipes [23]

The first of these methods is the most reliable; however, it may not be viable for all applications, particularly pipelines located in remote or submerged locations. Flow channels could be operated with inhibitor injection at the well, with dehydration of the flow occurring further downstream to solve. Compared with the flexible pipe analysis described above, the research of hydrate formation in flexible pipes is an area that has not seen the same amount of study. As such, no papers could be found looking specifically at the effect hydrates have on flexible pipes. Most of the current research is based on how hydrates form in multi-phase flow. Some experimental work has been undertaken on this topic but has proved relatively unsuccessful, primarily due to the complexity and unpredictability of hydrate formation. Key elements of the practical work, which informed assumptions made for this paper, are discussed below.

Samim, Soroush Zarinabadi and Amir

The paper discussed the problems gas hydrate cause in the oil and gas industry which may increase

pipeline explosion if not prevented, using Iran as an example. One of the issues discussed is flow assurance; when oil is transported from the wellhead to the production site, if the temperature and pressure fall within the hydrate forming region, hydrate particles could start to form. They could eventually plug the pipeline, as shown in Figure 42.

Figure 42: Hydrate formation in the natural gas pipeline [33]

Hydrate blockages can cause production stoppages for months at a time, so it is advisable not to let them reach this stage. Hydrate propagation forms a plug that splits the pipe into two pressure sections: a high pressure, upstream section, between the wellhead and the plug, and low pressure, downstream section, between the plug and the production vessel. In this high-pressure section, a blast can occur in the pipe due to pressure growth. The plug, therefore, has the potential to destroy the pipe if the pressure difference between the high and low-pressure sections becomes too large, endangering personal safety and expensive production. A typical burst pipe on hydrate formation and eliminating clogging pipes with time is presented in Figures 43 and 44, respectively.

Figure 43: (a) Burst pipes on hydrate formation (b) Eliminating clogging in pipes [33]

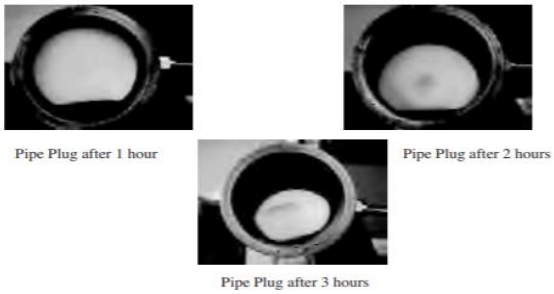

Figure 44: Eliminating clogging pipes with time [34]

FINITE ELEMENT ANALYSIS

Abaqus is used to model a complete finite element model of a hydrate blocked flexible pipe by parametric methodology. The non-bonded flexible pipe samples retrieved from a field in the Gulf of Guinea is studied and the parameter used in this research is derived from it as provided in the manufacturer manual.

The 6" gas injection flowline that was blocked by hydrate plug sometimes in the year 2010. The affected flowline was discovered after a comprehensive Remote Operated Vehicle (ROV) survey. The damaged section as shown in the diagram below, was identified on flowline (FL2) RG1 system (6" Gas Injection Line between FPSO and the wellhead) and located at 1097m from the Xmas tree.

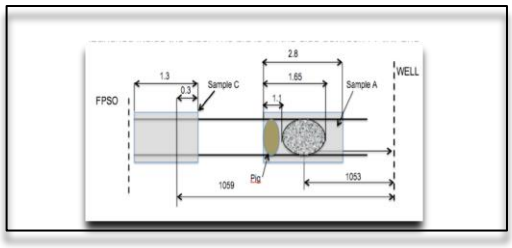

(a) [16]

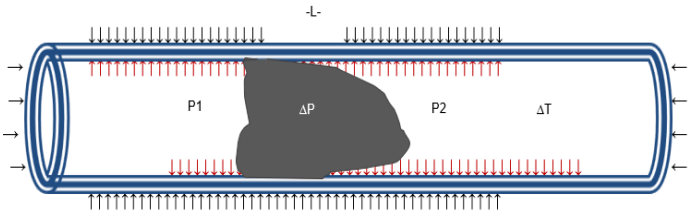

(b)

Figure 45: (a)- Schematic diagram of the flexible pipe under investigation (b)- Pressure application

Prior to the rupture, there was a blockage along the line and first attempt to unblock the line was successful through pressurization and depressurization. Subsequent blockages and removal through the same means, however, were not successful and attempts eventually led to the rupture of the flowline.

It is therefore envisaged that the fault may have been as a result of continuous pressurization and depressurization during pigging process.

The pipe under investigation has an inner and outer diameter of 152.4mm and 193.3mm respectively with 7-layers. The flexible pipe was simulated considering the contacts interfaces, interaction, and constriction. In this paper, coefficient of friction is assumed to be frictionless and, in some cases, it is varied, and the contact normal behavior is assumed to be linear with stiffness value of 0.0001.

The non-metallic layers; Pressure Sheath, High Strength Tape and Outer Sheath were modeled isotropic material created in a global cylindrical coordinate system with its origin located at the center of the flexible pipe end. The metallic parts; Carcass, Pressure Armour and Tensile wires were created by using equivalent materials for Carcass and Pressure Armour in orthogonal using engineering constants while Tensile wires were revolved with a rectangular end shape. All were modeled in solid element C3D8R reduced integration solid elements with number of elements and nodes used.

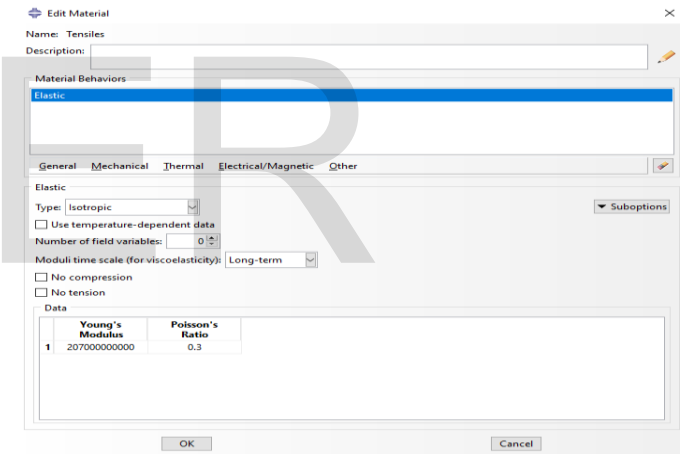

Figure 46: Material properties of Non-Metallic Part

The Carcass layers and Pressure armour layer are modeled using equivalent material even though they are steel build-up layers. Ideally, steel materials are not anisotropic thus; properties such as young's modulus should not change with direction along the axis. However, since these layers are built to resist hoops stress, they are wrapped in unique orientations and lay angles and their strengths are also determined by this.

The stress strain relationship was used as given by [1].

$$\alpha_{sx} = \frac{E_{sx}}{1-v_{sxy}V_{syx}}\varepsilon_{sx} + \frac{E_{sx}v_{syx}}{1-v_{sxy}V_{syx}}\varepsilon_{sy} \quad \text{Equation 12}$$

$$\alpha_{sy} = \frac{E_{sy}V_{syx}}{1-v_{sxy}V_{syx}}\varepsilon_{sx} + \frac{E_{sy}}{1-v_{sxy}V_{syx}}\varepsilon_{sy} \quad \text{Equation 13}$$

Consequently, $\tau_{syx} = G_{syx}y_{syx}$

Where $\alpha_{s,}$ τ, ε_s and Ys are the normal and shear stress at the shell surface, elongation, and angular distortion respectively. Es, Gs and Vs are represented as the Young's modulus, Shear modulus and Poison's ratio of the shell material respectively. Since the tendons do not resist loads normal to lay direction according to hypotheses, it is assumed that *Esx=o and Vsyx=Vsxy=o*. Thus; $\alpha_{sx} = E_{sx}\varepsilon_{sx}$ $\alpha_{sy} = 0$ $\tau_{sxy} = G_{sx}y_{sxy}$

The membrane, torsional stiffness and bending of an orthotropic shell element are given in the equation below:

$$(EA)s = hsEsx \qquad (EI)s = \left(\frac{H^3s}{12}\right)E \qquad (GJ)s = \left(\frac{h^3s}{3}\right)\text{Gsxy} \quad \text{Equation 14}$$

Where *hs* is the shell thickness of the plate theory (Woinowsky-Krieger, 1959). The axial, bending and torsional stiffness of a helical tendon is further given by;

$$(EA)t = \left(\frac{A*nt}{Lp}\right)E \qquad (EI)t = \left(\frac{Ieq*nt}{Lp}\right)E \qquad (GJ)t = \left(\frac{J*nt}{Lp}\right)G \quad \text{Equation 15}$$

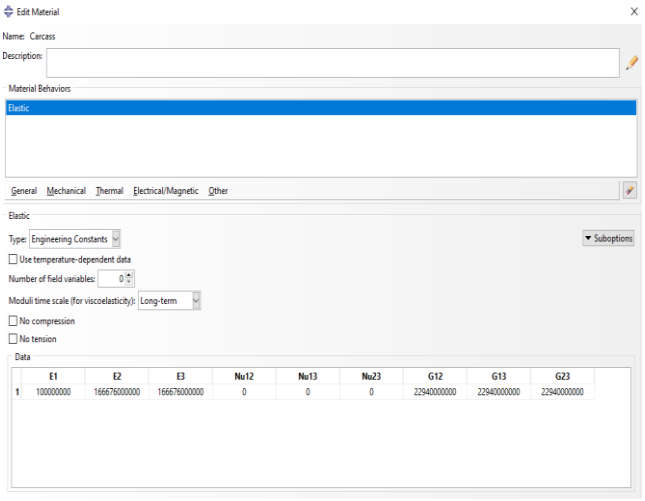

Figure 47: Material properties of Metallic Part

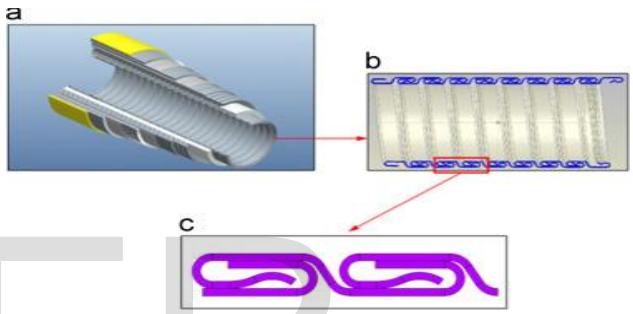

Figure 48: Carcass and Pressure Sheath configuration

The non-flexible layers and the material properties are shown in the table below after adopting the equivalent materials for Carcass and Pressure Armour as used by [1]. The layers were modelled in SOLID/SHELL Element, Extrusion and Deformable and tensile wires modelled in revolution; the layers:

1. Carcass
2. Pressure Sheath
3. Zeta/Pressure Armour
4. 1st Tensile Armour
5. 2nd Tensile Armour
6. High Strength Tape
7. Outer Sheath

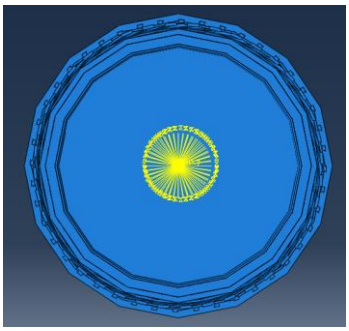

Figure 49: Configuration of Flexible layers

The length of the modelled pipe was 2.8 meters to limit the computation times. The Blockage/Plug presented is composed of methane hydrate properties of young modules 8.52GPa.

Geometry

A hypothetical 6" (152.4mm) flexible pipe was developed for the analysis. The basic geometric properties for all the layers including the pipe layer specification and material properties that are detailed in the table below:

Element and General Mesh

The typical finite element mesh of the individual flexible pipe layers is shown below with global seeds of approximately global size curvature control of maximum deviation factor of 0.1 and minimum size control by fraction of global size 0.1 applied. This was applied to all the seven (7) layers including the plug/blockage.

The effect of different element sizes in the cross-section of the pipe layers were examined to provide accurate results at a reduced computation time.

In order to get accurate and better results, the layer parts were finely meshed and observed. The number of elements were carefully chosen, so that the aspect ratio of the elements was as close to one as possible. Therefore, mesh sensitivity analyses were performed to verify the number of elements in each of the parts. All the layers were modelled in 8-noded SOLID C3D8R.

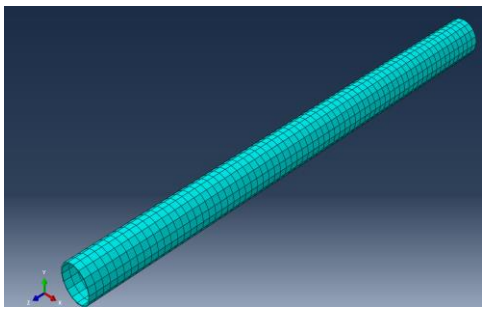

Figure 50: A meshed part

DEVELOPING THE METALLIC PARTS

Tensile Armours

The tensile wires are modelled as solid, which is deformable and revolution, it revolves from a sketch of the tendon of a considerable cross section. In the modelling of the wires, the part was created using the cross-sectional dimensions as given by the manufacturer that has a sectional dimension of (2 x 7) mm tendon sketched and the mid-point is taken from the distance equal to the mean radius of the layer of the pipe.

For the parts, the tensile wires were represented by Solid Continuum 3D 8 nodes reduced elements (C3D8R).

It starts with creating part where 3D, Deformable and Revolution options were selected under modelling space, part type and base feature point respectively.

The wires were then made from coordinates using rectangular shape with the dimension 2 x 7 mm and material properties of carbon steel assigned

tendons. The material orientation is assigned with discrete options to get accurate stress and displacement sizes. On the primary axis, direction 1 is used and direction 3 was chosen for Normal axis and defined as normal to the wire surfaces.

However, in the revolve dialogue window, the move sketch normal to path option is selected and the wires cross section is revolved based on an angle and pitch. The pitch is half the length of other parts as considered for both inner and outer tensile wires. Though, the outer tensile wires length may be deviated slightly from the inner tensile wires in order to coincide with the length of the other parts in the model.

Instances are created in the assembly module with radial patterns based on the number of strand of wires which in this model is 44 wires. The angle is set to 360° and the tensile wires created along the pipe longitudinal axis.

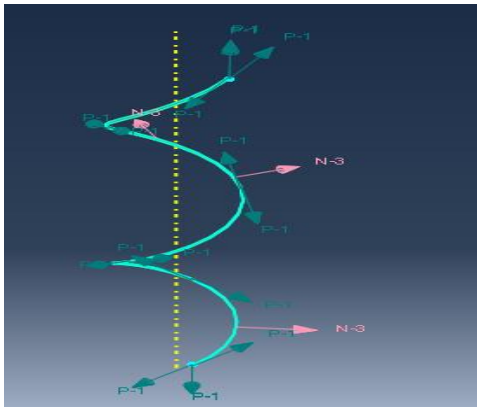

Figure 51: tendon of tensile wires representing a pitch and its orientation

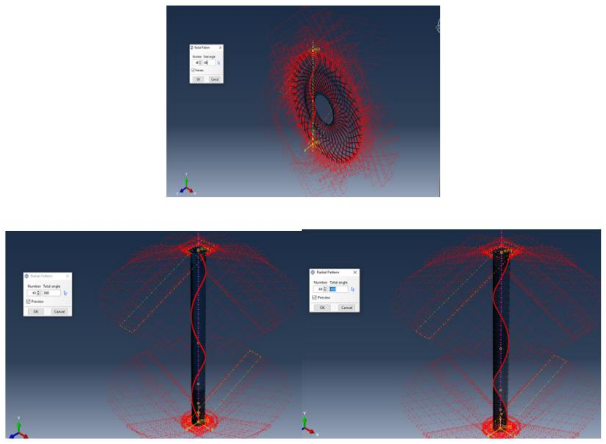

(a) First tensile wire (b) Second tensile wire

Figure 52: 40 tendons of first tensile and 44 tendons of second tensile wire

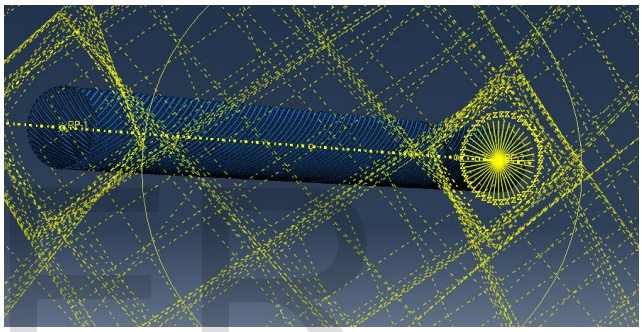

Figure 53: Inner Tensile wire

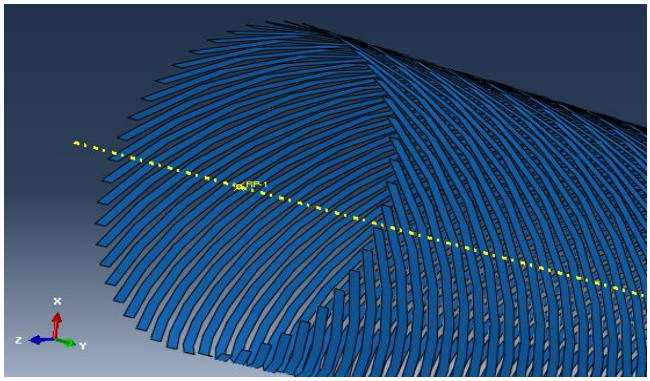

Figure 54: a complete tensile wire armour

Carcass and Pressure Armour

Carcass and Pressure armour layers are helically wrapped with small angles (long pitch) to support axial loads for the amours. When the layers are helically wrapped with high angles (short pitch), they tend to establish resistance to hoop stress due

to internal and external pressure and this is mostly concentrated on the carcass and pressure armour. In other to simulate an exact or near layer-behaviour of both layers, an equivalent material property was developed. The postulations used in this development was based on established standard procedure and theory of [1]. The layers are represented by C3D8R which is similar to the non-metallic parts (Pressure Sheath, High Strength Tape and External Sheath). Orthotropic materials, engineering constants were used for carcass/pressure armour while isotropic materials properties were used for the tape and sheaths layers. The equivalent material properties were developed by considering the angle of lay of both carcass and pressure armour layers. This study provides a background understanding of lay angle application and how its features is introduced in orthotropic materials (engineering constant) within the Abaqus CAE environment.

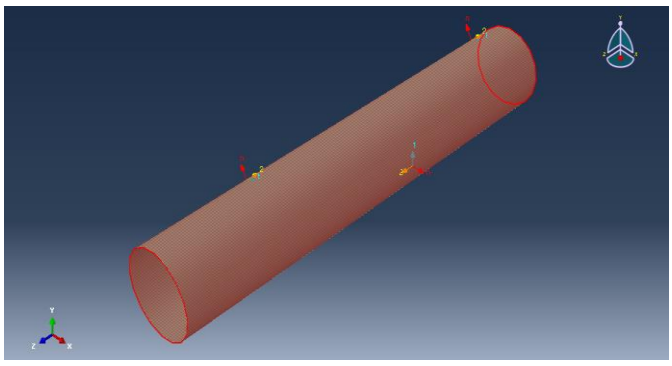

Figure 55: Carcass

DEVELOPING THE NON-METALLIC PARTS

The Pressure sheath, High Strength Tape and outer sheath layers are modeled individually as simply cylindrical hollow pipe.

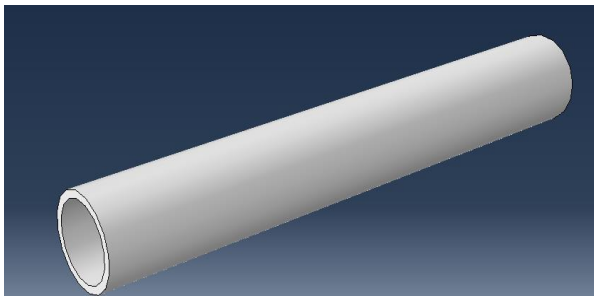

Figure 56: showing non-metallic part

PIPE PROPERTIES

A hypothetical 6" flexible pipe was developed for the analysis. The basic geometric properties for all the layers including the pipe layer specification and material properties are detailed in the table below:

Table 3: 7-Layers 6" Non-Bonded Flexible Pipe

No. Layer description	I.D. (mm)	h (mm)	E (MPa)	v	I.R (m)	O.R (m)
Interlocked Carcass 48.0 X 1.0 AISI 304 (Fe 02)	160.05	1.17	165065	0	0.08003	0.0812
RILSAN P40tl Tp01 Pressure Sh.	162.40	6.42	800	0.4	0.0812	0.08762
Zeta Wire Th. 6.0 FM 35 (Fi 11)	175.23	3.78	136919	0	0.08762	0.0914
First Armour Lay 35.0 Deg. High Character. Fi41 (2x7) 44 wires	182.80	2.00	207000	0.3	0.0914	0.0934
Second Armour Lay -35.0 Deg. High Character. Fi41 (2x7) 44 wires	186.80	2.00	207000	0.3	0.0934	0.0954
High Strength Tape 1 Tape (BA09 KV 400dab,130 Mm)	190.80	1.25	112000	0.35	0.0954	0.09665
External Sheath FINATHENE (TP 04)	193.30	4.80	800	0.4	0.09665	0.10145

Properties

As stated in the table, the values of the equivalent materials for carcass and pressure armour in terms of the young modulus E and shear modulus G are calculated as shown below.

Table 4: Carcass and Pressure Armour Equivalent Properties

Carcass				Pressure Armour				Poisson's Ratio
	MPa		MPa		MPa		MPa	
E1	100000	G1	22940	E1	100000	G1	84605	0
E2	165065	G2	22940	E2	136919	G2	84605	0
E3	165065	G3	22940	E3	136919	G3	84605	0

So, with De Sousa, 2009 [2] principle based on the equation detailed above, the equivalent materials for the Carcass and Pressure armour were calculated and that what gave rise to the new diameter and thickness of carcass and pressure armour as shown in the property table.

Hydrate Plug Properties and Dimension

A complete blockage modelled with the materials of methane hydrate is used and presented in table 5.
The mechanical behaviour of this model has been evaluated under three loading conditions; tension force, internal and external pressure.

Table 5: Blockage (Plug) Properties

Length (m)	Inner diameter (mm)	Modulus (GPa)	Poisson's ratio	Density (kg/m^3)
1.0	0.0762	8.65	0.38	2,500

INTERACTIONS AND CONSTRAINTS

General contact algorithm in Abaqus/Standard explicit which is surface to surface contact formulation was used for all layers except the tensile wires that interacts with self. Two surfaces, surf 1 and surf 2 were created each for the parts and the contact domain contain surface pairs of a master and a slave. It is therefore important to note that the metallic parts were all made masters while the non-metallic are slaves, this is to protect unnecessary absorption. For the numerical simulations, it is normal behavior, pressure overclosure: hard contact, constraint enforcement method by default and allow separation after contact was adopted. Otherwise, pressure overclosure: Linear, constraint enforcement method by default with contact stiffness of 10^{-5} was adopted while in tangential behavior, friction formulation: frictionless was used.

The penalty algorithm was used for both normal and

tangential directions in which the contact stiffness factor is calculated (i.e., in normal direction) based on penetration of the master surface into the slave surface.

LOAD AND BOUNDARY CONDITIONS

The ends boundary conditions were imposed through reference points RP1 and RP2 located at both ends of the pipe segment. One end RP1 is constrained at all points while RP2 free. Coupling the end nodes of the elements in six degrees of freedom with the reference node simulated the axial and radial constraint of the end fitting.

At end 1, the layers were constrained in all direction using Encastre while at End 2, the layers are constrained to a reference point RP2 and it is free.

Loading Cases

Load case investigates the influence of the following loads for the two samples:

Internal pressure

- Operating Pressure 22.7MPa
- Design Pressure 27.6MPa
- Factory Test Pressure 41.4MPa
- Burst Pressure 65.4MPa

Subsequently, for these load cases, the essential boundary conditions were to define one end fixed while the other pipe end was free.

BLOCKAGE SIMULATION

A complete blockage of tangential behaviour, penalty, and normal behaviour of stiffness constant 10^{-5} shows a significant decrease in the displacement and high stress concentration in all direction in the flexible pipe.

It is clearly shown that the plug in the flexible impart more mises stress, reacting force and hoop stress on the entire structure that resulted into bird cage and twist in the tensile wires with eventual collapse and burst.

RESULTS AND DISCUSSION

The Stress analyses are performed for Sample A and Sample B blocked and unblocked flexible pipe specimens. The numerical investigation is to confirm certain properties as stated by the pipe manufacturer. This includes but not limited to the following [16]:

- Pressure Nominal Bursting- 65.4MPa
- Hydrostatic Collapse Pressure- 11.7 MPa
- Operating Pressure 22.7MPa
- Design Pressure 27.6MPa
- Factory Test Pressure 41.4MPa
- Damaging pull in a straight line- 1747.79 kN

This is carried out under same conditions for the models. The concentration of stress in the layers particularly the two tensile wires are critically studied. Internal pressure 22.7MPa was applied at the inner surface of the carcass and on the hydrate plug for Sample A. The stress analyses are performed with the boundary conditions and loads described earlier.

The analysis shows that the layers in Sample A particularly the tensile wires are highly sensitive to the applied load. This results into large deformation even with smaller load. However, the deformation in Sample B is not as noticeable as in Sample A being that the pipe is operating under normal conditions.

Flexible Pipes Under Investigation

- Sample A (Blocked/ Damaged)
- Sample B (Unblocked/Not Damaged)

The pipes were modeled to determine their behaviour under the same load conditions. It is noted that the stress concentration on the two pipe models vary from one layer to another.

The models are verified by comparing their stress, displacement and axial load impacted by the blockage (Plug).

The responses of the pipes to the subject load shows a significant deformation in Sample A which indicates the presence of the plug in the pipe triggers one of the failure modes stated in API 17B.

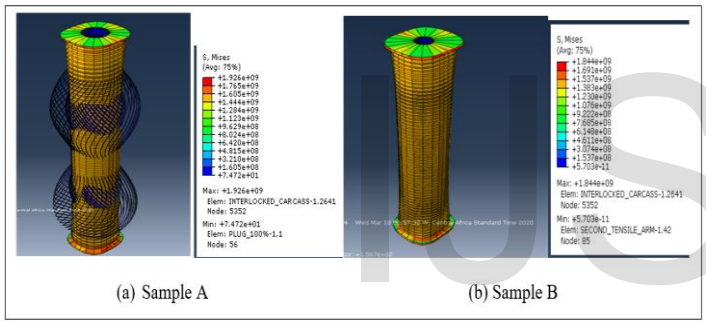

Figure 57: (a) & (b) shows the deformation of Sample-A and Sample-B under Internal Pressure

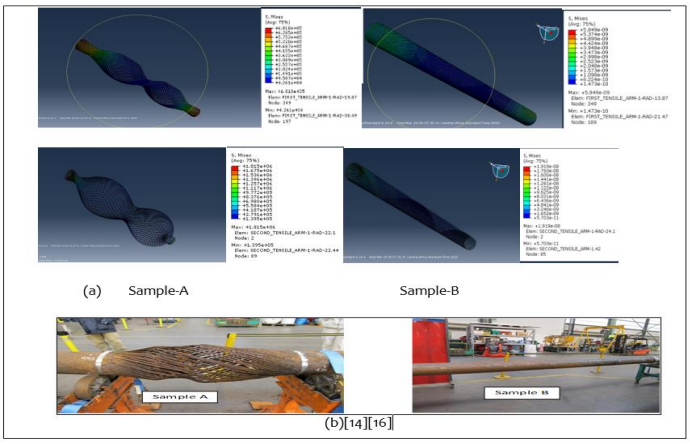

Figure 58: a- represents Sample A and Sample B first and second Tensile wires deformation under internal pressure while b- represents pipe under investigation

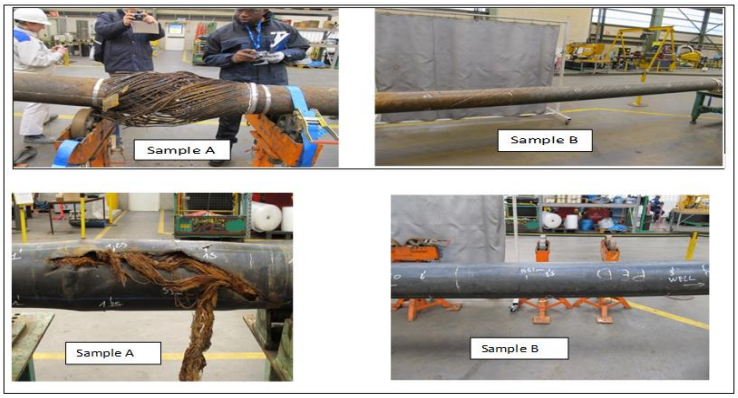

Figure 59: Pipe under investigation with the same deformation with simulated pipes [14]

COMPARISON OF CRITICAL LOADS

Sample A and Sample B

Load case: Internal Pressure- the load 22.7MPa is applied on the inner surface of the carcass and the hydrate plug of about 1m long inside the flexible pipe. However, the deformation of the hydrate blocked flexible pipe was conspicuous. The first tensile wire was twisted at the middle and the ends, the deformation at the two points of first tensile wire resembles a bird cage that is ready to burst. The second tensile wire also look like a balloon ready to burst and resemble the first tensile wire deformation.

The unblocked pipe showed little deformation along the pipe except the carcass that is deformed like the shape of the first tensile wire. Values of stress concentration is higher in the blocked pipe while it is almost negligible on the unblocked pipe. This is expected as the unblocked pipe is operating under normal design pressure 27.6MPa. The maximum stress distribution on each layer S_{mises} and S_{22} is shown in table 6 where 1.93GPa and 1.84GPa are the

maximum stress on Sample-A and Sample B respectively. It is good to see that Sample B values of stresses and displacement reflects good results that indicates good condition under operating pressure.

Table 6: Computation Results of Hoop Stress using (a) Lame's (b) Normal Equations

No. Layer description	Internal Pressure (P) (MPa)	Inner Radius (Ri) (m)	Outer Radius (Ro) (m)	Hoop Stress (H_s) (MPa)
Interlocked carcass	22.7	0.0800	0.0812	1559

(a) Lame's

No. Layer description	Internal Pressure (P) (MPa)	Inner Diameter (d) (m)	thickness (t) (m)	Hoop Stress (H_s) (MPa)
Interlocked carcass	22.7	0.1601	0.0012	1514

(b) Normal

Table 7: Comparation of Hoop Stress

No. Layer description	Internal Pressure (P) (MPa)	Hoop Stress (H_s) (MPa)		
		Abaqus Model	Lamis' Equation	Normal Equation
Interlocked carcass	22.7	1574	1559	1514

The tables 6 with the summary in on table 7 shows a close hoop stress values for Carcass layer. The result of the model is approximately the same as the calculated value of the hoop stress, and that the model is valid. It is worth noting that further refining the quality of the mesh will give a more accurate result which may even be closer to the theoretical value.

BEHAVIOURAL PLOT OF THE SAMPLES UNDER LOAD CONDITIONS

The stress distribution in the layers of the samples under consideration is shown in Figure 60 for carcass and Figure 61 for Zeta layer. The sinusoidal in Zeta layer sample B shows normal behaviour while in sample A indicates deviation or issues. Carcass conditions for both samples show deviations because the internal pressure load is placed directly on the layer surface and resulted in excess stress concentration.

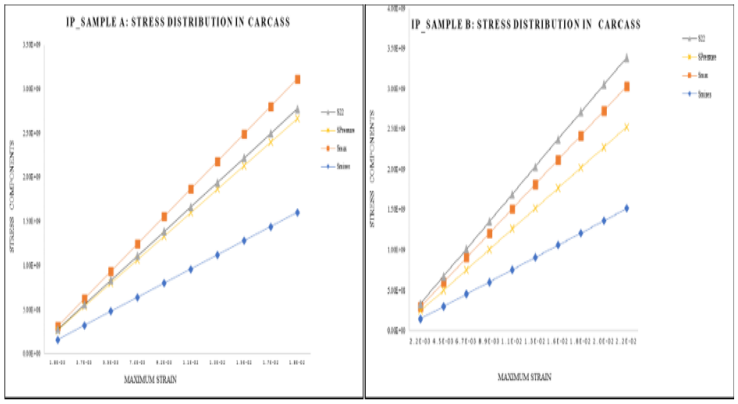

Figure 60: Stress distribution in Carcass-Sample A & B subjected to Internal Pressure

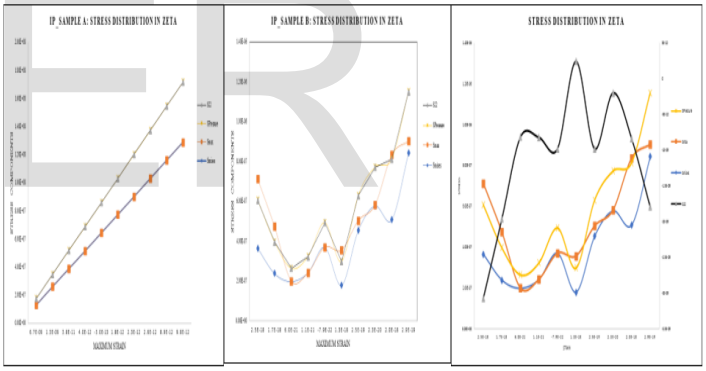

Figure 61: Stress distribution in Zeta (Pressure Armour)-Sample A & B subjected to Internal Pressure

RECOMMENDATION AND CONCLUSION

The results obtained and the deformation of Sample A, showed the effects of pigging of pipeline under hydrate blockage should not be neglected. The layers observed are highly sensitive to the load most especially the carcass and the tensile wires.

The stress concentrations and values are greater in the blocked pipe while it is almost negligible in the unblocked pipe.

Conclusively, it is recommended that blocked pipe should be handled by carefully consider manufacturer procedure, standard bodies requirement and operating manual when undergoing pigging or during any attempt to remove the blockage by any means. If, not carefully handled might cause permanent deformation of the flexible pipe and perhaps may need to be replaced spending several millions of dollars if anything goes wrong.

Further works are recommended to determine other conditions that could affect the pipes when operating under loads, this is to eliminate those conditions that can cause damage to the pipe and adopt suitable methods for the removal and cleaning of the flexible pipes. This is to avoid burst and collapse of the pipes under environmental and internal conditions.

REFERENCES

[1] Witz, J. A. and Tan, Z. (1992) 'On the Structural Behavior of Flexible pipes, Umbilical's and Marine Cables', *Marine Structures*, 5(2–3), pp. 205–227. doi: 10.1016/0951-8339(92)90029

[2] De Sousa, J. R. M., Magluta, C., Roitman, N., et al., 2009. "On the Response of Flexible Risers to Loads Imposed by Hydraulic Collars," Applied Ocean Research, 31, pp. 157-170.

[3] API, July 2008, Specification for Unbonded Flexible Pipe, API RP 17J, American Petroleum Institute, 3rd ed, New York.

[4] API, July 2008, Recommended Practice for Flexible Pipe, API RP 17B, American Petroleum Institute, 4th ed, New York

[5] Brandt, Ulrikke, Prof. Svein Sævik, P. J. R. (2014) 'Impact Analysis of Flexible Riser', *Master's Thesis in the International Master's Programme Naval Architecture and Ocean Engineering*.

[6] Nygård, D. and Saevik, S. (2012) 'Tensile armour buckling in flexible pipes', (June),mp.71. Available at: https://daim.idi.ntnu.no/masteroppgaver/007/7612/masteroppgave.pdf.

[7] Gabriel Gonzalez, Jose Renato and Mendes des Sousa in the paper, *A non-bonded flexible pipe finite element model*

[8] Larsen, C. M. (1992) 'Flexible Riser Analysis - Comparison of Results from Computer Program', *Marine Structures*, 5(2–3), pp. 103–119. doi: 10.1016/0951-8339(92)90024-J.

[9] Sævik, S. (1993) 'A Finite Element Model For Predicting Stresses and Slip In Flexible Pipe Armouring Tendons', *Computers and Structures*, 46(2), pp. 219–230. doi:10.1016/0045-7949(93)90187-I.

[10] Sævik, S. (2011) 'Theoretical and Experimental Studies of Stresses In Flexible Pipes', *Computers and Structures*, 89(23–24), pp. 2273–2291. doi: 10.1016/j.compstruc.2011.08.008.

[11] De Sousa, J. R. M. *et al.* (2012) 'An Experimental and Numerical Study on the Axial Compression Response of Flexible Pipes', *Journal of Offshore Mechanics and Arctic Engineering*, 134(3), p. 031703. doi: 10.1115/1.4005181.

[12] Svein Sævik (2010) 'Comparison Between Theoretical and Experimental Flexible Pipe Bending Stresses', *Proceedings of the ASME 2010 29th International Conference on Ocean, Offshore and Arctic Engineering*, OMAE2010(20352), pp. 6–13.

[13] Kvenvolden, K.A..L., 2001. The global occurance of natural gas hydrate. *Natural Gas Hydrates: Occurance, Distribution and detection*, pp.3-18.

[14] I Clement, E Godefroy and others, 2014 Abo 5 6" GI flowline expertise and failure analysis_ 26_05_2014.

[15] Alfano, G., Bahtui, A. and Bahai, H. (2009) 'Numerical Derivation of Constitutive Models for Non bonded Flexible Risers', *International Journal of Mechanical Sciences*, 51(4), pp. 295–304. doi: 10.1016/j.ijmecsci.2009.02.002.

[16] ENI flexible pipe final workshop 26.05.2014 POLIMI.

[17] Ben Edmans, Dinh Chi Pham, Zhiqian Zhang, Tianfu Guo, Sridhar Narayanaswamy, G. S. (2014) 'Multiscale Finite Element Analysis of Non bonded Flexible Risers', *Proceedings of the ASME 2014 33rd International Conference on Ocean, Offshore and Arctic Engineering*, OMAE2014-2, pp. 1–9.

[18] Edmans, B. (2013) 'Non-Linear Finite Element Analysis of Flexible Pipes for Deep-Water Applications', (March). Available at: https://core.ac.uk/download/pdf/29410157.pdf.

[19] Eduardo Ribeiro Malta, C. de A. M. (2014) 'Finite Element Analysis of Flexible Pipes Under Compression', *Proceedings of the ASME 2014 33rd International Conference on Ocean, Offshore and Arctic Engineering*, OMAE2014, pp. 1–11.

[20] Leroy, J.-M. and Estrier, P. (2001) 'Calculation of Stresses and Slips In Helical Layers of Dynamically Bent Flexible Pipes', *Oil & Gas Science and Technology – Rev. IFP*, 56(6), pp. 545–554. doi: 10.2516/ogst:2001044.

[21] Li, J. Y., Qiu, Z. X. and Ju, J. S. (2015) 'Numerical Modeling and Mechanical Analysis of Flexible Risers', 2015.

[22] O.A. Bauchau, J. I. C. (2009) *Structural Analysis*, *Springer*. doi: 10.1007/978-90-481-2516-6.

[23] Oñate, E. (2009) *Structural Analysis with the Finite Element method. Linear Statics. Volume 1. Basis and Solids*, *Structural Analysis with the Finite Element Method*. doi: 10.1007/978-1-4020-8733-2_1.

[24] Ostergaard, N. H., Lyckegaard, A. and Andreasen, J. H. (2012) 'On Modelling of Lateral Buckling Failure in Flexible Pipe Tensile Armour Layers', *Marine Structures*. Elsevier Ltd, 27(1), pp. 64–81. doi: 10.1016/j.marstruc.2012.03.005.

[25] Østergaard, N. H., Lyckegaard, A. and Andreasen, J. H. (2011) 'Simulation of Frictional Effects In Models For Calculation of The Equilibrium State of Flexible Pipe Armouring Wires In Compression and Bending', *Rakenteiden Mekaniikka (Journal of Structural Mechanics)*, 44(3), pp. 243–259. Available at: http://rmseura.tkk.fi/rmlehti/2011/nro3/RakMek_44_3_2011_7.pdf.

[26] Perdrizet, T. *et al.* (2011) 'Stresses In Armour Layers of Flexible Pipes : Comparison of Abaqus Models', *SIMULIA Customer Conference*, pp. 1–14.

[27] Ren, S. Fei, Tang, W. Yong and Guo, J. ting (2014) 'Behavior of Non bonded Flexible Risers Subject to Axial Tension', *China Ocean Engineering*, 28(2), pp. 249–258. doi: 10.1007/s13344-014-0020-9.

[28] Tan, Z., Quiggin, P. and Sheldrake, T. (2007) 'Time Domain Simulation of the 3d Bending Hysteresis Behaviour of a Non bonded Flexible Riser', *Proceedings of the 26th International Conference on Offshore Mechanics and Arctic Engineering*, OMAE2007(29315).

[29] Vargas-Londoño, T. *et al.* (2014) 'A Theoretical and Experimental Analysis of The Bending Behavior of Non bonded Flexible Pipes', *Proceedings of the ASME 2014 33rd International Conference on Ocean, Offshore and Arctic Engineering*, Omae2014(24247), pp. 1–11.

[30] Liu, Z. Study of hydrate deposition and sloughing of gas- dominated pipelines using numerical and analytical models. PhD Thesis, Colorado School of Mines, US, 2017.

[31] Simulia. ABAQUS 16.4-4 Online Documentation. http://abaqus.software.polimi.it/v6.14/index.html

[32] Gonzalez, G. M., De Sousa, J. R. M., Sagrilo, L.V.S., An unbonded flexible pipe finite element model. In Proceedings of 36th Ibero-Latin America Congress on Computational Methods in Engineering, Rio de Janeiro, 22-25 November 2015.

[33] Bai, Y., Bai, Q. Subsea Pipelines and Risers. ELSEVIER Ltd, 2005, pp 497- 499.